



1 **Impacts of microtopographic snow-redistribution and lateral subsurface processes**
2 **on hydrologic and thermal states in an Arctic polygonal ground ecosystem**

3
4 **Gautam Bisht¹, William J. Riley¹, Haruko M. Wainwright¹, Baptiste Dafflon¹, Yuan**
5 **Fengming², and Vladimir E. Romanovsky³**

6
7 ¹Climate & Ecosystem Sciences Division, Lawrence Berkeley National Laboratory, 1
8 Cyclotron Road, Berkeley, California 94720, USA

9
10 ²Environmental Sciences Division, Oak Ridge National Laboratory, Oak Ridge, TN, 37831-
11 6301, USA

12
13 ³Geophysical Institute, University of Alaska Fairbanks, Fairbanks, AK 99775, USA

14
15 Correspondence to: Gautam Bisht (gbisht@lbl.gov)

16
17 **Abstract**

18 Microtopographic features, such as polygonal ground, are characteristic sources of
19 landscape heterogeneity in the Alaskan Arctic coastal plain. Here, we analyze the effects of
20 snow redistribution (SR) and lateral subsurface processes on hydrologic and thermal states
21 at a polygonal tundra site near Barrow, Alaska. We extended the land model integrated in
22 the ACME Earth System Model (ESM) to redistribute incoming snow by accounting for
23 microtopography and incorporated subsurface lateral transport of water and energy
24 (ALMv0-3D). Three 10-years long simulations were performed for a transect across
25 polygonal tundra landscape at the Barrow Environmental Observatory in Alaska to isolate
26 the impact of SR and subsurface process representation. When SR was included, model
27 results show a better agreement (higher R^2 with lower bias and RMSE) for the observed
28 differences in snow depth between polygonal rims and centers. The model was also able to
29 accurately reproduce observed soil temperature vertical profiles in the polygon rims and
30 centers (overall bias, RMSE, and R^2 of 0.59°C, 1.82°C, and 0.99, respectively). The spatial
31 heterogeneity of snow depth during the winter due to SR generated surface soil



32 temperature heterogeneity that propagated in depth and time and led to ~10 cm shallower
33 and ~5 cm deeper maximum annual thaw depths under the polygon rims and centers,
34 respectively. Additionally, SR led to spatial heterogeneity in surface energy fluxes and soil
35 moisture during the summer. Excluding lateral subsurface hydrologic and thermal
36 processes led to small effects on mean states but an overestimation of spatial variability in
37 soil moisture and soil temperature as subsurface liquid pressure and thermal gradients
38 were artificially prevented from spatially dissipating over time. The effect of lateral
39 subsurface processes on active layer depths was modest with mean absolute difference of
40 ~3 cm. Our integration of three-dimensional subsurface hydrologic and thermal subsurface
41 dynamics in the ACME land model will facilitate a wide range of analyses heretofore
42 impossible in an ESM context.

43 **1 Introduction**

44 The northern circumpolar permafrost region, which contains ~1700 Pg of organic
45 carbon down to 3 m (Tarnocai et al., 2009), is predicted to experience disproportionately
46 larger future warming compared to the tropics and temperate latitudes (Holland and Bitz,
47 2003). Recent warming in the Arctic has led to changes in lake area (Smith et al., 2005),
48 snow cover duration and extent (Callaghan et al., 2011a), vegetation cover (Sturm et al.,
49 2005), growing season length (Smith et al., 2004), thaw depth (Schuur et al., 2008),
50 permafrost stability (Jorgenson et al., 2006), and land-atmosphere feedbacks (Euskirchen
51 et al., 2009). Future predictions of Arctic warming include northward expansion of shrub
52 cover in tundra (strum 2001, Tape et al 2006), decreases in snow cover duration
53 (Callaghan et al., 2011a), and emissions of CO₂ and CH₄ from decomposition of
54 belowground soil organic matter (Koven et al., 2011; Schaefer et al., 2011; Schuur and
55 Abbott, 2011, Xu, 2016 #154; Xu et al., 2016).

56 Several recent modeling studies have predicted a positive carbon-climate feedback
57 at the global scale (Cox et al., 2000; Dufresne et al., 2002; Friedlingstein et al., 2001; Fung et
58 al., 2005; Govindasamy et al., 2011; Jiang et al., 2011; Jones et al., 2003; Koven et al., 2015;
59 Matthews et al., 2007b; Matthews et al., 2005; Sitch et al., 2008; Thompson et al., 2004;
60 Zeng et al., 2004), although the strength of this predicted feedback at the year 2100 was



61 shown to have a large variability across models (Friedlingstein et al., 2006). In contrast to
62 the ocean carbon cycle, the terrestrial carbon cycle is expected to be a more dominant
63 factor in the global carbon-climate feedback over the next century (Matthews et al., 2007a;
64 Randerson et al., 2015).

65 Changes in Arctic ecosystem net ecosystem productivity (NEP, defined as the
66 difference between net primary production (NPP) and heterotrophic respiration (R_h)) will
67 be determined by the magnitude and direction of changes in NPP and R_h . Warming
68 experiments in the Arctic have found increases and decreases of plant growth in response
69 to higher temperatures (Barber et al., 2000; Chapin et al., 1995; Cornelissen et al., 2001;
70 Hobbie and Chapin, 1998; Hollister et al., 2005; Van Wijk et al., 2004; Walker et al., 2006;
71 Wilmking et al., 2004). Arctic ecosystems are limited in nitrogen availability (Schimel et al.,
72 1996; Shaver and Chapin III, 1986) and higher mineralization rates under warmer climate
73 (Hobbie, 1996) could lead to higher CO_2 fixation by plants (Shaver and Chapin, 1991).
74 Additionally, a longer growing season is expected to result in a negative carbon-climate
75 feedback by increasing NPP (Euskirchen et al., 2006). On the other hand, microbial
76 decomposition of previously frozen soil organic matter under a warmer climate is expected
77 to strengthen the carbon-climate feedback (Davidson and Janssens, 2006; Mack et al., 2004;
78 Oechel et al., 1993; Tarnocai et al., 2009).

79 Snow, which covers the Arctic ecosystem for 8-10 months each year (Callaghan et
80 al., 2011b), is a critical factor influencing hydrologic and ecologic interactions (Jones,
81 1999). Snowpack modifies surface energy balances (via high reflectivity), soil thermal
82 regimes (due to low thermal conductivity), and hydrologic cycles (because of melt water).
83 Several studies have shown that warm soil temperatures under snowpack support the
84 emission of greenhouse gases from belowground respiration (Grogan and Chapin Iii, 1999;
85 Sullivan, 2010) and nitrogen mineralization (Borner et al., 2008; Schimel et al., 2004)
86 during winter. Additionally, decreases in snow cover duration have been shown to increase
87 net ecosystem CO_2 uptake (Galen and Stanton, 1995; Groendahl et al., 2007). Recent snow
88 manipulation experiments in the Arctic have provided evidence of the importance of snow
89 in the expected responses of Arctic ecosystems under future climate change (Morgner et al.,
90 2010; Nobrega and Grogan, 2007; Rogers et al., 2011; Schimel et al., 2004; Wahren et al.,
91 2005; Welker et al., 2000).



92 Apart from the spatial extent and duration of snowpack, the spatial heterogeneity of
93 snow depth is an important factor in various terrestrial processes (Clark et al., 2011;
94 Lundquist and Dettinger, 2005). The spatial distribution of snow not only affects the
95 quantity of snowmelt discharge (Hartman et al., 1999; Luce et al., 1998), but also the water
96 chemistry (Rohrbough et al., 2003; Wadham et al., 2006; Williams et al., 2001). Lawrence
97 and Swenson (2011) demonstrated the importance of snow depth heterogeneity in
98 predicting responses of the Arctic ecosystem to future climate change by performing
99 idealized numerical simulations of shrub expansion across the pan-Arctic region using the
100 Community Land Model (CLM4). Their results showed that an increase in active layer
101 thickness (ALT) under shrubs was negated when spatial heterogeneity in snow cover due
102 to wind driven snow redistribution was accounted for, resulting in an unchanged grid cell
103 mean active layer thickness. López-Moreno et al. (2014) identified processes responsible
104 for snow depth heterogeneity at three distinct spatial scales: microtopography at 1-10 m
105 (Lopez-Moreno et al., 2011); wind induced lateral transport processes at 100-1000 m
106 (Liston et al., 2007); and precipitation variability at catchment scales of 10 – 1000 km
107 (Sexstone and Fassnacht, 2014).

108 Large portions of the Arctic are characterized by polygonal ground features, which
109 are formed in permafrost soil when frozen ground cracks due to thermal contraction
110 during winter and ice wedges form within the upper several meters (Hinkel et al., 2005).
111 Polygons can be classified as ‘low-centered’ or ‘high-centered’ based on the relationship
112 between their central and mean elevations. Polygonal ground features are dynamic
113 components of the Arctic landscape in which the upper part of ice-wedge thaw under low-
114 centered polygon troughs leads to subsidence, eventually (~o(centuries)) converting the
115 low-centered polygon into a high-centered polygon (Seppala et al., 1991). Microtopography
116 of polygonal ground influences soil hydrologic and thermal conditions (Engstrom et al.,
117 2005). In addition to controlling CO₂ and CH₄ emissions, soil moisture affects (1)
118 partitioning of incoming radiation into latent, sensible, and ground heat fluxes (Hinzman
119 and Kane, 1992; McFadden et al., 1998); (2) photosynthesis rates (McGuire et al., 2000;
120 Oberbauer et al., 1991; Oechel et al., 1993; Zona et al., 2011); and (3) vegetation
121 distributions (Wiggins, 1951).



122 Our goals in this study include (1) analyzing the effects of spatially heterogeneous
123 snow in polygonal ground on soil temperature and moisture and surface processes (e.g.,
124 surface energy budgets); (2) analyzing how model predictions are affected by inclusion of
125 lateral subsurface hydrologic and thermal processes; and (3) developing and testing a
126 three-dimensional version of the land model ALM (Tang and Riley, 2016; Zhu and Riley,
127 2015) integrated in the ACME Earth System Model (ESM). We note that the original version
128 of ALM is equivalent to CLM4.5 (Koven et al., 2013; Oleson, 2013a), and represents vertical
129 energy and water dynamics, including phase change. We expanded on that model to
130 explicitly represent soil lateral energy and hydrological exchanges and fine-resolution
131 snow redistribution (ALMv0-3D). We then applied ALMv0-3D to a transect across a
132 polygonal tundra landscape at the Barrow Environmental Observatory in Alaska. After
133 defining our study site, the model improvements, model tests against observations, and
134 analyses, we apply the model to examine the effects of snow redistribution and lateral
135 subsurface processes on snow micro-topographical heterogeneity, soil temperature, and
136 the surface energy budget.

137 **2 Methodology**

138 **2.1 Study Area**

139 Our analysis focuses on sites located near Barrow, Alaska (71.3° N, 156.5° W) from
140 the long term Department of Energy (DOE) Next-Generation Ecosystem Experiment (NGEE-
141 Arctic) project. The four primary NGEE-Arctic study sites (A, B, C, D) are located within the
142 Barrow Environmental Observatory (BEO), which is situated on the Alaskan Coastal Plain.
143 The annual mean air temperature for our study sites is approximately -13°C (Walker et al.,
144 2005) and mean annual precipitation is 106 mm with the majority of precipitation
145 occurring during the summer season (Wu et al., 2013). The study site is underlain with
146 continuous permafrost (Brown et al., 1980) and the annual maximum thaw depth (active
147 layer depth) ranges between 30-90 cm (Hinkel et al., 2003). Although the overall
148 topographic relief for the BEO is low, the four NGEE study sites have distinct
149 microtopographic features: low-centered (A), high-centered (B), and transitional polygons
150 (C, D). Contrasting polygon types are indicative of different stages of permafrost



151 degradation and were the primary motivation behind the choice of study sites for the
152 NGEE-Arctic project. LIDAR Digital Elevation Model (DEM) data were available at 0.25 m
153 resolution for the region encompassing all four NGEE sites. In this work, we perform
154 simulations along a two-dimensional transect in low-centered polygon Site-A as shown by
155 the dotted line in Figure 1.

156 2.2 ALMv0 Description

157 We developed the capability to represent three-dimensional hydrology and thermal
158 dynamics in ALMv0 (Zhu et al., 2016b), and call the new model ALMv0-3D. ALMv0 was
159 derived from CLM4.5 (Ghimire et al., 2016; Koven et al., 2013), and is the land model
160 integrated in the ACME Earth System Model (ESM). The model represents coupled plant
161 biophysics, soil hydrology, and soil biogeochemistry (Oleson *et al.* 2013). We run ALMv0-
162 3D here with prescribed plant phenology (called Satellite Phenology (SP) mode), since our
163 focus is on the thermal dynamics of the system, rather than the C cycle dynamics.

164 2.3 Representing Two- and Three-Dimensional Physics

165 2.3.1 Subsurface hydrology

166 The flow water in the unsaturated zone is given by the θ -based Richards equations
167 as

$$\frac{\partial \theta}{\partial t} = -\nabla \cdot \vec{q} - Q \quad (1)$$

168 where θ [m^3m^{-3}] is the volumetric soil water content, t [s] is time, \vec{q} [ms^{-1}] is Darcy flux, and
169 Q [m of water m^{-3} of soil s^{-1}] is volumetric sink of water. Darcy flux is given by

$$\vec{q} = -k\nabla(\psi + z) \quad (2)$$

170 where k [ms^{-1}] is the hydraulic conductivity and ψ [m] is the soil matric potential. The
171 hydraulic conductivity and soil matric potential are non-linear functions of volumetric soil
172 moisture. ALMv0 uses the modified form of Richards equation of Zeng and Decker (2009)
173 that computes Darcy flux as

$$\vec{q} = -k\nabla(\psi + z - C) \quad (3)$$

174 where C is a constant hydraulic potential above the water table, z_v , given as



$$C = \psi_E + z = \psi_{sat} \left[\frac{\theta_E(z)}{\theta_{sat}} \right]^{-B} + z = \psi_{sat} + z_V \quad (4)$$

175 where ψ_E [m] is the equilibrium soil matric potential. Substituting equations (3) and (4)
 176 into equation (1) yields the equation for the vertical transport of water in ALMv0:

$$\frac{\partial \theta}{\partial t} = \frac{\partial}{\partial z} \left[k \left(\frac{\partial(\psi - \psi_E)}{\partial z} \right) \right] - Q \quad (5)$$

177 A finite volume spatial discretization and implicit temporal discretization with Taylor
 178 series expansion leads to a tri-diagonal system of equations. We extended this 1-D Richards
 179 equation to a 3-D representation integrated in ALMv0-3D, which is presented next.

180 We use a cell-centered finite volume discretization to decompose the spatial domain
 181 into N non-overlapping control volumes, Ω_n , such that $\Omega = \bigcup_{n=1}^N \Omega_n$ and Γ_n represents the
 182 boundary of the n -th control volume. Applying a finite volume integral to equation (1) and
 183 the divergence theorem yields

$$\frac{\partial}{\partial t} \int_{\Omega_n} \theta dV = - \int_{\Gamma_n} (\vec{q} \cdot d\vec{A}) - \int_{\Omega_n} Q dV \quad (6)$$

184 The spatially discretized equation for the n -th grid cell that has V_n volume and n' neighbors
 185 is given by

$$\frac{d\theta_n}{dt} V_n = - \sum_{n'} (\vec{q}_{nn'} \cdot \vec{A}_{nn'}) - Q V_n \quad (7)$$

186 For the sake of simplicity in presenting the discretized equation, we assume the 3-D grid is
 187 a Cartesian grid with each grid cell having a thickness of Δx , Δy , and Δz in the x , y , and z
 188 directions, respectively. Using an implicit time integral, the 3-D discretized equation at time
 189 $t + 1$ for a (i, j, k) control volume is given as

$$\begin{aligned} \left(\frac{\Delta \theta_{i,j,k}^{t+1}}{\Delta t} \right) V_{i,j,k} = & \left(q_{x_{i-1/2,j,k}}^{t+1} - q_{x_{i+1/2,j,k}}^{t+1} \right) \Delta y \Delta z \\ & + \left(q_{y_{i,j-1/2,k}}^{t+1} - q_{y_{i,j+1/2,k}}^{t+1} \right) \Delta x \Delta z \\ & + \left(q_{z_{i,j,k-1/2}}^{t+1} - q_{z_{i,j,k+1/2}}^{t+1} \right) \Delta x \Delta y - Q V_{i,j,k} \end{aligned} \quad (8)$$

190 where q_x , q_y and q_z are Darcy flux in the x , y , and z directions, respectively and $\Delta \theta_{i,j,k}^{t+1}$ is the
 191 change in volumetric soil liquid water in time Δt . Using the same approach as Oleson



192 (2013b), the Darcy flux in all three directions is linearized about θ using Taylor series
 193 expansion. The linearized Darcy flux in the x direction at the $(i - 1/2, j, k)$ interface is a
 194 function of $\theta_{i-1,j,k}$ and $\theta_{i,j,k}$:

$$q_{x_{i-1/2,j,k}}^{t+1} = q_{x_{i-1/2,j,k}}^t + \frac{\partial q_{x_{i-1/2,j,k}}^t}{\partial \theta_{i-1,j,k}} \Delta \theta_{i-1,j,k}^{t+1} + \frac{\partial q_{x_{i-1/2,j,k}}^t}{\partial \theta_{i,j,k}} \Delta \theta_{i,j,k}^{t+1} \quad (9)$$

195 The linearized Darcy fluxes in the y and z directions are computed similarly. Substituting
 196 equation (9) in equation (8) results in a banded matrix of the form

$$\alpha \Delta \theta_{i-1,j,k}^{t+1} + \beta \Delta \theta_{i,j-1,k}^{t+1} + \gamma \Delta \theta_{i,j,k-1}^{t+1} + \eta \Delta \theta_{i+1,j,k}^{t+1} + \mu \Delta \theta_{i,j+1,k}^{t+1} + \phi \Delta \theta_{i,j,k+1}^{t+1} + \zeta \Delta \theta_{i,j,k}^{t+1} = \varphi \quad (10)$$

197 where α , β , and γ are subdiagonal entries; η , μ , and ϕ are superdiagonal entries; ζ is
 198 diagonal entry of the banded matrix; and φ is a column vector given by

$$\alpha = \frac{\partial q_{x_{i-1/2,j,k}}^t}{\partial \theta_{i-1,j,k}} \Delta y \Delta z \quad (11)$$

$$\beta = \frac{\partial q_{y_{i,j-1/2,k}}^t}{\partial \theta_{i,j-1,k}} \Delta x \Delta z \quad (12)$$

$$\gamma = \frac{\partial q_{z_{i,j,k-1/2}}^t}{\partial \theta_{i,j,k-1}} \Delta x \Delta y \quad (13)$$

$$\eta = \frac{\partial q_{x_{i+1/2,j,k}}^t}{\partial \theta_{i+1,j,k}} \Delta y \Delta z \quad (14)$$

$$\mu = \frac{\partial q_{y_{i,j+1/2,k}}^t}{\partial \theta_{i,j+1,k}} \Delta x \Delta z \quad (15)$$

$$\phi = \frac{\partial q_{z_{i,j,k+1/2}}^t}{\partial \theta_{i,j,k+1}} \Delta x \Delta y \quad (16)$$

$$\zeta = \left(\frac{\partial q_{x_{i-1/2,j,k}}^t}{\partial \theta_{i,j,k}} - \frac{\partial q_{x_{i+1/2,j,k}}^t}{\partial \theta_{i,j,k}} \right) \Delta y \Delta z + \left(\frac{\partial q_{y_{i,j-1/2,k}}^t}{\partial \theta_{i,j,k}} - \frac{\partial q_{y_{i,j+1/2,k}}^t}{\partial \theta_{i,j,k}} \right) \Delta x \Delta z + \left(\frac{\partial q_{z_{i,j-1/2,k}}^t}{\partial \theta_{i,j,k}} - \frac{\partial q_{z_{i,j+1/2,k}}^t}{\partial \theta_{i,j,k}} \right) \Delta x \Delta y - \frac{\Delta x \Delta x \Delta z}{\Delta t} \quad (17)$$



$$\begin{aligned} \varphi = & - \left(q_{x_{i-\frac{1}{2},j,k}}^t - q_{x_{i+\frac{1}{2},j,k}}^t \right) \Delta y \Delta z - \left(q_{y_{i,j-\frac{1}{2},k}}^t - q_{y_{i,j+\frac{1}{2},k}}^t \right) \Delta x \Delta z \\ & - \left(q_{z_{i,j-\frac{1}{2},k}}^t - q_{z_{i,j+\frac{1}{2},k}}^t \right) \Delta x \Delta y + Q_{i,j,k}^{t+1} \Delta x \Delta x \Delta z \end{aligned} \quad (18)$$

199 The coefficients of equation (10) described in equation (11)-(18) are for an internal grid
 200 cell with six neighbors. The coefficients for the top and bottom grid cells are modified for
 201 infiltration and interaction with the unconfined aquifer in the same manner as Oleson
 202 (2013b). Similarly, the coefficients for the grid cells on the lateral boundary are modified
 203 for a no-flux boundary condition. See Oleson (2013b) for details about the computation of
 204 hydraulic properties and derivative of Darcy flux with respect to soil liquid water content.

205 2.3.2 Subsurface thermal

206 ALMv0 solves a tightly coupled system of equations for soil, snow, and standing
 207 water temperature (Oleson, 2013a). The model solves the transient conservation of energy:

$$c \frac{\partial T}{\partial t} = -\nabla \cdot F \quad (19)$$

208 where c is the volumetric heat capacity [$\text{J m}^{-3} \text{K}^{-1}$], F is the heat flux [W m^{-2}], and t is time
 209 [s]. The heat conduction flux is given by

$$F = -\lambda \nabla T \quad (20)$$

210 where λ is thermal conductivity [$\text{W m}^{-1} \text{K}^{-1}$] and T is temperature [K]. Applying a finite
 211 volume integral to equation (20) and divergence theorem yields

$$c \frac{\partial}{\partial t} \int_{\Omega_n} T = - \int_{\Gamma_n} \vec{F} \cdot d\vec{A} \quad (21)$$

212 The spatially discretized equation for a n -th grid cell that has V_n volume and n' neighbors is
 213 given by

$$c_n \frac{dT_n}{dt} V_n = - \sum_{n'} (\vec{F}_{nn'} \cdot \vec{A}_{nn'}) \quad (22)$$

214 Similar to the approach taken in Section 2.3.1, ALMv0-3D assumes a 3-D Cartesian grid
 215 with each grid cell having a thickness of Δx , Δy , and Δz in the x , y , and z directions,
 216 respectively. Temporal integration of equation (22) is carried out using the Crank-
 217 Nicholson method that uses a linear combination of fluxes evaluated at time t and $t + 1$:



$$\begin{aligned}
 c_n \frac{(T_{i,j,k}^{t+1} - T_{i,j,k}^t)}{\Delta t} \Delta x \Delta y \Delta z &= \omega \left\{ (F_{x_{i-1/2,j,k}}^t - F_{x_{i+1/2,j,k}}^t) \Delta y \Delta z \right. \\
 &+ (F_{y_{i,j-1/2,k}}^t - F_{y_{i,j+1/2,k}}^t) \Delta x \Delta z \\
 &+ (F_{z_{i,j,k-1/2}}^t - F_{z_{i,j,k+1/2}}^t) \Delta x \Delta y \left. \right\} \\
 &+ (1 - \omega) \left\{ (F_{x_{i-1/2,j,k}}^{t+1} - F_{x_{i+1/2,j,k}}^{t+1}) \Delta y \Delta z \right. \\
 &+ (F_{y_{i,j-1/2,k}}^{t+1} - F_{y_{i,j+1/2,k}}^{t+1}) \Delta x \Delta z \\
 &+ (F_{z_{i,j,k-1/2}}^{t+1} - F_{z_{i,j,k+1/2}}^{t+1} + 1) \Delta x \Delta y \left. \right\} \quad (23)
 \end{aligned}$$

218 where ω is the weight in the Crank-Nicholson method and set to 0.5 in this study.

219 Substituting a discretized form of heat flux using equation (20) in equation (23), results in

220 a banded matrix of the form

$$\begin{aligned}
 \alpha T_{i-1,j,k}^{t+1} + \beta T_{i,j-1,k}^{t+1} + \gamma T_{i,j,k-1}^{t+1} + \eta T_{i+1,j,k}^{t+1} + \mu T_{i,j+1,k}^{t+1} + \phi T_{i,j,k+1}^{t+1} + \zeta \Delta T_{i,j,k}^{t+1} \\
 = \varphi \quad (24)
 \end{aligned}$$

221 where α , β , and γ are subdiagonal entries; η , μ , and ϕ are superdiagonal entries; ζ is

222 diagonal entry of the banded matrix; and φ is a column vector given by

$$\alpha = \left(\frac{-\omega' \Delta t}{c_{i,j,k} \Delta x} \right) \left(\frac{\lambda_{i-1/2,j,k}}{x_{i,j,k} - x_{i-1,j,k}} \right) \quad (25)$$

223

$$\beta = \left(\frac{-\omega' \Delta t}{c_{i,j,k} \Delta y} \right) \left(\frac{\lambda_{i,j-1/2,k}}{y_{i,j,k} - y_{i-1,j,k}} \right) \quad (26)$$

224

$$\gamma = \left(\frac{-\omega' \Delta t}{c_{i,j,k} \Delta z} \right) \left(\frac{\lambda_{i,j,k-1/2}}{z_{i,j,k} - z_{i,j,k-1}} \right) \quad (27)$$

225

$$\mu = \left(\frac{-\omega' \Delta t}{c_{i,j,k} \Delta x} \right) \left(\frac{\lambda_{i+1/2,j,k}}{x_{i+1,j,k} - x_{i,j,k}} \right) \quad (28)$$

226

$$\xi = \left(\frac{-\omega' \Delta t}{c_{i,j,k} \Delta y} \right) \left(\frac{\lambda_{i-1/2,j,k}}{y_{i+1,j,k} - y_{i,j,k}} \right) \quad (29)$$



227

$$\phi = \left(\frac{-\omega' \Delta t}{c_{i,j,k} \Delta Z} \right) \left(\frac{\lambda_{i-1/2,j,k}}{z_{i+1,j,k} - z_{i,j,k}} \right) \quad (30)$$

228

$$\begin{aligned} \zeta = 1 + & \left(\frac{\omega' \Delta t}{c_{i,j,k} \Delta x} \right) \left[\frac{\lambda_{i-1/2,j,k}}{x_{i,j,k} - x_{i-1,j,k}} + \frac{\lambda_{i+1/2,j,k}}{x_{i+1,j,k} - x_{i,j,k}} \right] \\ & + \left(\frac{\omega' \Delta t}{c_{i,j,k} \Delta y} \right) \left[\frac{\lambda_{i,j-1/2,k}}{y_{i,j,k} - y_{i-1,j,k}} + \frac{\lambda_{i-1/2,j,k}}{y_{i+1,j,k} - y_{i,j,k}} \right] \\ & + \left(\frac{\omega' \Delta t}{c_{i,j,k} \Delta z} \right) \left[\frac{\lambda_{i,j,k-1/2}}{z_{i,j,k} - z_{i,j,k-1}} + \frac{\lambda_{i-1/2,j,k}}{z_{i+1,j,k} - z_{i,j,k}} \right] \end{aligned} \quad (31)$$

229

$$\begin{aligned} \varphi = T_{i,j,k}^t + & \left(\frac{\omega \Delta t}{c_{i,j,k} \Delta x} \right) (F_{x_{i-1/2,j,k}}^t - F_{x_{i+1/2,j,k}}^t) \\ & + \left(\frac{\omega \Delta t}{c_{i,j,k} \Delta y} \right) (F_{y_{i,j-1/2,k}}^t - F_{y_{i,j+1/2,k}}^t) \\ & + \left(\frac{\omega \Delta t}{c_{i,j,k} \Delta z} \right) (F_{z_{i,j,k-1/2}}^t - F_{z_{i,j,k+1/2}}^t) \end{aligned} \quad (32)$$

230 The coefficients of equation (24) described in equation (25)-(32) are for an internal grid
 231 cell with six neighbors. The coefficients for the top and bottom grid cells are modified for
 232 presence of snow and/or standing water, and no-flux boundary. The coefficients for the
 233 grid cells on the lateral boundary are modified for a no-flux boundary condition. ALM
 234 handles ice-liquid phase transitions by first predicting temperatures at the end of a time
 235 step and then updating temperatures after accounting for deficits or excesses of energy
 236 during melting or freezing. See Oleson (2013b) for details about the computation of
 237 thermal properties and phase transition.

238 2.3.3 Numerical solution via PETSc

239 ALMv0, which considers flow only in the vertical direction, solves a tridiagonal and
 240 banded tridiagonal system of equations for water and energy transport, respectively. In
 241 ALMv0-3D, accounting for lateral flow in the subsurface results in a sparse linear system,
 242 equations (10) and (24), where the sparsity pattern of the linear system depends on grid
 243 cell connectivity. In this work, we use the PETSc (Portable, Extensible Toolkit for Scientific



244 Computing) library (Balay et al., 2016) developed at the Argonne National Laboratory to
245 solve the sparse linear systems. PETSc provides object-oriented data structures and solvers
246 for scalable scientific computation on parallel supercomputers.

247 **2.4 Snow Model and Redistribution**

248 The snow model in ALMv0-3D is the same as that in the default ALMv0 and CLM4.5
249 (Anderson, 1976; Dai and Zeng, 1997; Jordan, 1991). The snow model allows for a dynamic
250 snow depth and up to 5 snow layers, and explicitly solves the vertically-resolved mass and
251 energy budgets. Snow aging, compaction, and phase change are all represented in the snow
252 model formulation. Additionally, the snow model accounts for the influence of aerosols
253 (including black and organic carbon and mineral dust) on snow radiative transfer (Oleson,
254 2013a). ALMv0 uses the methodology of Swenson and Lawrence (2012) to compute
255 fractional snow cover area, which is appropriate for ESM-scale grid cells (~100 [km] x 100
256 [km]). Since the grid cell resolution in this work is sub-meter, we modified the fractional
257 cover to be either 1 (when snow was present) or 0 (when snow was absent). Two main
258 drivers of snow redistribution (SR) include topography and surface wind (Warscher et al.,
259 2013); previous SR models include mechanistically- (Bartelt and Lehning, 2002; Liston and
260 Elder, 2006) and empirically- (Frey and Holzmann, 2015; Helfricht et al., 2012) based
261 approaches. To mimic the effects of wind, we used a conceptual model to simulated SR over
262 the fine-resolution topography of our site by instantaneously re-distributing the incoming
263 snow flux such that lower elevation areas (polygon center) receive snow before higher
264 elevation areas (polygon rims). This relatively simple and parsimonious approach is
265 reasonable given the observed snow depth heterogeneity, as described below, and small
266 spatial extent of our domain.

267 **2.5 System Characterization**

268 Hydrologic and thermal properties differ by depth and landscape type. We used the
269 horizontal distribution of OM organic matter from Wainwright et al. (2015) to infer soil
270 hydrologic and thermal properties following the default representations in ALM.
271 Vegetation cover was classified as arctic shrubs in polygon centers and arctic grasses in
272 polygon rims. The default representation of the plant wilting factor assigns a value of zero



273 for a given soil layer when its temperature falls below a threshold ($T_{\text{threshold}}$) of $-2\text{ }^{\circ}\text{C}$. This
274 default value leads to overly large predicted latent and sensible heat fluxes during winter,
275 compared to nearby eddy covariance measurements. We modified $T_{\text{threshold}}$ to be $0\text{ }^{\circ}\text{C}$ in this
276 study, resulting in improved predicted wintertime latent heat fluxes compared to the
277 default version of the model (**Error! Reference source not found.**). Although biases
278 compared to the observations remain, particularly for sensible heat fluxes in the spring, the
279 improvement is substantial and, given the observational uncertainties, we believe sufficient
280 to justify our use of the model for investigations of the role of snow heterogeneity in this
281 polygonal tundra system.

282 2.6 Simulation Setup, Climate Forcing, and Analyses

283 Because of computational constraints, we investigated the role of snow
284 redistribution and physics representation using a two-dimensional transect through site A
285 (Figure 1). The transect was 104 [m] long and 45 [m] deep that was discretized
286 horizontally with a grid spacing of 0.25 [m] and an exponentially varying layer thickness in
287 the vertical with 30 soil layers. No flow conditions for mass and energy were imposed on
288 the east, west, and bottom boundaries of the domain. Temporal discretization of 30 [min]
289 was used in the simulations. All simulations were performed in “SP” mode, i.e., Leaf Area
290 Index (LAI) was prescribed from MODIS observations.

291 Simulations were run for 10 years using long-term climate data gathered at the
292 Barrow, Alaska Observatory site (<https://www.esrl.noaa.gov/gmd/obop/brw/>) managed
293 by the Global Monitoring Division of NOAA’s Earth System Research Laboratory (Mefford et
294 al., 1996). The missing precipitation time series was gap-filled using daily precipitation at
295 the Barrow Regional Airport available from the Global Historical Climatology Network
296 (<http://www1.ncdc.noaa.gov/pub/data/ghcn/daily>). We tested the model by comparing
297 predictions to high-frequency observations of snow depth and vertically resolved soil
298 temperature for September 2012 – September 2013. Temperature observations were
299 taken at discrete locations in a polygon center and rim (Figure 1), and were combined to
300 analyze comparable landscape positions in the simulations (Figure 2).

301 After testing, the model was used to investigate the effect of snow redistribution and
302 2D subsurface hydrologic and thermal physics by analyzing three scenarios: (1) no snow



303 redistribution and 1D physics; (2) snow redistribution and 1D physics; and (3) snow
304 redistribution and 2D physics. Between these scenarios, we compared vertically-resolved
305 soil temperature and liquid saturation, active layer depth, and mean and spatial variation of
306 latent and sensible heat fluxes across the 10 years of simulations. For each soil column, the
307 simulated soil temperature was interpolated vertically and the active layer depth was
308 estimated as the maximum depth that had above-freezing soil temperature.

309 **3 Results and Discussion**

310 **3.1 Snow depth**

311 In the absence of SR, predicted snow depth exactly follows the topography. With SR,
312 a much larger dependence of winter-average snow depth on topography is predicted
313 (Figure 2). Further, for the winter average, there are very small differences in snow depth
314 between simulations with SR and 1D or 2D subsurface physics representations. Compared
315 to observations, considering snow redistribution led to: (1) a factor of ~ 2 improvement in
316 snow depth bias for the polygon center; (2) modest increase and decrease in average bias
317 on the rims for September through February and March through June, respectively; and (3)
318 a dramatic improvement in bias of the difference in snow depth between the polygon
319 centers and rims (Figure 3). There was no discernible difference in snow depth bias
320 between the 1D and 2D physics (Table 1), although the predicted subsurface temperature
321 fields were different, as shown below.

322 The temporal variation of the mean snow depth (**Figure 4a**) and its spatial standard
323 deviation (**Figure 4b**) also differed based on whether SR was considered, but was not
324 affected by considering 2D thermal or hydrologic physics. With SR, the snow depth
325 coefficient of variation (**Figure 4c**) was about 0.5 from December through the beginning of
326 the snowmelt period, indicating relatively large spatial heterogeneity. Snapshots of
327 simulated snow depth for the three simulation scenarios are included in Supplementary
328 material (**Error! Reference source not found.**).



329 3.2 Soil Temperature and Active Layer Depth

330 Broadly, ALMv0-3D accurately predicted the polygon center soil temperature at
331 depth intervals corresponding to the temperature probes (0-20 cm, 20-50 cm, 50-75 cm,
332 and 75-100 cm; Figure 5a). Recall that the observed temperatures for the polygon center
333 and rims were taken at single points in site A (Figure 1) while the predicted temperatures
334 were calculated as averages across the transect for each of the two landscape position
335 types. The model was able to simulate early freeze up of the soil column under the rims as
336 compared to centers in November 2012 because of differences in accumulated snow pack.
337 The transition to thawed soil in the 0-20 cm depth interval in early June 2013 and the
338 subsequent temperature dynamics over the summer were very well captured by ALMv0-
339 3D. Minimum temperatures during the winter were also accurately predicted, although the
340 temperatures in the deepest layer (75-100 cm) were overestimated by $\sim 3^{\circ}\text{C}$ in March. For
341 figure clarity we did not indicate the standard deviation of the observations, but provide
342 that information in Supplemental Material (**Error! Reference source not found. - Error!**
343 **Reference source not found.**).

344 Similarly, the soil temperatures were accurately predicted in the polygon rims
345 (Figure 5b). The largest discrepancies between measured and predicted soil temperatures
346 were in the shallowest layer (0 - 25 cm), where the predictions were up to a few $^{\circ}\text{C}$ cooler
347 than some of the observations between December 2012 and March 2013. In the polygon
348 center, a thicker snow pack acts as a heat insulator and keeps soil temperature higher in
349 winter as compared to the polygon rims.

350 Three recent studies have used other mechanistic models to simulate the soil
351 temperature fields at this site, and achieved comparably good comparisons with the
352 observations (Kumar et al. 2016 applied a 3D version of PFLOTRAN; Atchley et al. 2015 and
353 Harp et al. 2016 applied a 1D version of ATS). However, those models used the measured
354 soil temperature near the surface as the top boundary condition. In contrast, the top
355 boundary condition in this work is the climate forcing (air temperature, wind, solar
356 radiation, humidity, precipitation), and the ground heat flux is prognosed based on ALM's
357 vegetation and surface energy dynamics. We note that no parameter calibration was done



358 in this work or that of Kumar et al. (2016), while the ATS parameterizations were tuned to
359 match the soil temperature profile.

360 Snow redistribution impacts spatial variability of soil temperature throughout the
361 soil column. Absence of SR results in no significant spatial variability of soil temperature
362 (Figure 6a). Inclusion of SR on the surface modifies the amount of energy exchanged
363 between the snow and the top soil layer, thereby creating spatial variability in the
364 temperature of the top soil, which propagates down into the soil column (Figure 6b). With
365 SR, energy dissipation in the lateral direction reduces the penetration depth of the soil
366 temperature spatial variance (compare Figure 6c and Figure 6b).

367 With 1D physics, the average spatial and temporal difference of the active layer
368 depth (ALD) between simulations with and without SR was 1.7 cm (Figure 7a), and the
369 absolute difference was 6.5 cm. As described above, we diagnosed the ALD to be the
370 maximum soil depth during the summer at which vertically interpolated soil temperature
371 is 0 °C. On average, the rims had ~10 cm shallower ALD with (blue line) than without
372 (green line) SR, consistent with the loss of insulation from SR on the rims during the
373 winter. In the centers (e.g., at location 42 - 55 m), the thaw depth was deeper by ~5 cm
374 with SR because of the higher snow depth there from SR. The effect of SR on the ALD was
375 largest on the rims because, compared to centers, they (1) on average lost more snow with
376 SR and (2) are more thermally conductive. Since rims are therefore colder at the time of
377 snowmelt with SR, the ground heat flux during the subsequent summer was unable to thaw
378 the soil column as deeply as when SR is ignored. For comparison, Atchley et al. (2015)
379 found in their sensitivity analysis using the 1D version of ATS that SR resulted in deeper
380 thaw depths in both polygon centers (by ~3 cm) and rims (~0.3 cm). Thus, there results for
381 polygon centers are consistent in sign but lower in magnitude than ours, but opposite in
382 sign for the rims.

383 Across ten years of simulation, the inter-annual variability (IAV) in ALD varied
384 substantially between the three scenarios (Figure 7b). As expected, for the 1D physics
385 without SR scenario (green line), the IAV in ALD was determined by landscape position
386 because of differences in soil and vegetation parameters. With SR and 1D physics, the
387 model shows largest differences over the rims, again highlighting the relatively larger
388 effects of SR on the rim soil temperatures.



389 The effect of 1D versus 2D physics on the ALD across the transect was modest
390 (mean absolute difference ~ 3 cm). Generally, because 2D physics allows for lateral energy
391 diffusion, the horizontal variation of ALD was slightly lower (i.e., the red line is smoother
392 than the blue line; Figure 7a) than with 1D physics. This difference was also reflected in the
393 thaw depth IAV across the transect, where 2D physics led to a smoother lateral profile of
394 inter-annual variability than with 1D physics.

395 The impact of physics formulation (i.e., 1D or 2D) alone was investigated by
396 analyzing differences between soil temperature profiles over time for polygon rims and
397 centers in simulations with snow redistribution. Inclusion of 2D subsurface physics
398 resulted in soil temperatures with depth and time that were lower in the polygon rims
399 (Figure 8a) and higher in polygon centers (Figure 8b). Using the simulations from the
400 scenario with SR and 2D physics, we evaluated the extent to which the soils under rims and
401 centers can be separately considered as relatively homogeneous single column systems by
402 evaluating the soil temperature standard deviation as a function of depth and time (Figure
403 9). During winter, both polygon rims and centers showed soil temperature spatial
404 variability > 1 °C up to a depth of ~ 2 [m]. The soil temperature spatial variability in winter
405 due to snow redistribution is dissipated over the summer. During the summer, polygon
406 centers were relatively more homogeneous vertically compared to polygon rims.

407 **3.3 Surface Energy Budget**

408 Predicted monthly- and spatial-mean (μ) surface latent heat fluxes across the
409 transect were very similar between the three scenarios (Figure 10a), with a growing
410 season mean difference of < 1.0 [$W m^{-2}$]. However, the spatial variability ($SV = \sigma$; Figure
411 10b) and coefficient of variation ($CV = \sigma/\mu$; Figure 10c) of latent heat fluxes were different
412 between the scenarios with SR (1D and 2D physics) and without SR. With SR, the latent
413 heat flux spatial standard deviation peaked after snowmelt and declined until the fall when
414 snow began, from about $\sim 100\%$ to 10% of the mean. This relatively larger spatial variation
415 in latent heat flux occurred because of large spatial heterogeneity in near surface soil
416 moisture in the beginning of summer, indicating a residual effect of SR from the previous
417 winter.



418 The predicted temporal monthly-mean and spatial-mean surface sensible heat
419 fluxes across the transect were also similar between the three scenarios (Figure 11a), with
420 a growing season mean absolute difference of $< 3.5 \text{ W m}^{-2}$. Also, the sensible heat flux
421 spatial variability differences occurred earlier than snowmelt, in contrast to the latent heat
422 flux. Both the standard deviation and CV of the sensible heat fluxes were larger than those
423 of the latent heat fluxes, with early season standard deviations of $\sim 50 \text{ W m}^{-2}$ (Figure 11b)
424 and CV's of ~ 1.5 (Figure 11c). As for the latent heat fluxes, the differences in standard
425 deviation and CV of sensible heat fluxes were small between the 1D and 2D scenarios with
426 SR, arguing that the subsurface lateral energy exchanges associated with the 2D physics did
427 not propagate to the mean surface heat fluxes. However, as for the latent heat flux, there
428 was a relatively large difference in spatial variation between the scenarios with and
429 without SR (e.g., of about 25 W m^{-2} in May; Figure 10b).

430 **3.4 Soil Moisture**

431 Neither SR nor 2D lateral physics affected the spatial mean moisture across time
432 (not shown). However, the spatial heterogeneity of predicted soil moisture content differed
433 substantially between scenarios during the snow free period (Figure 12). For the 1D
434 simulations, the effect of SR was to increase the growing season soil moisture spatial
435 heterogeneity by factors of 5.2 and 1.6 for 0-10 cm and 10-65 cm depth intervals,
436 respectively (compare Figure 12a and Figure 12b). Compared to the 1D physics, simulating
437 2D thermal and hydrologic physics led to an overall reduction in the soil moisture spatial
438 heterogeneity by factors of 0.8 and 0.7 for 0-10 cm and 10-65 cm depth intervals,
439 respectively (compare Figure 12b and Figure 12c). Thus, with respect to dynamic spatial
440 mean soil moisture, SR effects dominated those associated with lateral subsurface water
441 movement.

442 **3.5 Caveats and Future Work**

443 The good agreement between ALMv0-3D predictions and soil temperature
444 observations demonstrate the model's capabilities to represent this very spatially
445 heterogeneous and complex system. However, several caveats to our conclusions remain
446 due to uncertainties in model parameterizations, model structure, and climate forcing data.



447 Because of computational constraints, we applied a 2D transect domain to the site,
448 instead of a full 3D domain. We are working to improve the computational efficiency of the
449 model, which will facilitate a thorough analysis of the effects of 3D subsurface energy and
450 water fluxes. A related issue is our simplified treatment of surface water flows. A thorough
451 analysis of the effects of surface water redistribution would require integration of a 2D
452 surface thermal flow model with the ALMv0-3D in a 3D domain, which is another goal for
453 our future work. However, we note that the good agreement using the 2D model domain
454 supports the idea that a two-dimensional simplification may be appropriate for this system.
455 The expected geomorphological changes in these systems over the coming decades (e.g.,
456 Liljedahl et al. 2016), which will certainly affect soil temperature and moisture, are not
457 currently represented in ALM, although incorporation of these processes is a long-term
458 development goal.

459 The current representation of vegetation in ALMv0-3D for these polygonal tundra
460 systems is over-simplified. For example, non-vascular plants (mosses and lichens) are not
461 explicitly represented in the model, but can be responsible for a majority of evaporative
462 losses (Miller et al., 1976) and are strongly influenced by near surface hydrologic
463 conditions (Williams and Flanagan, 1996). Our use of the ‘satellite phenology’ mode, which
464 imposes transient LAI profiles for each plant functional type in the domain, ignores the
465 likely influence of nutrient constraints (Zhu et al., 2016a) on photosynthesis and therefore
466 the surface energy budget. Other model simplifications, e.g., the simplified treatment of
467 radiation competition may also be important, especially as simulations are extended over
468 periods where vegetation change may occur (e.g., Grant 2016).

469 **4 Summary and Conclusions**

470 We analyzed the effects of microtopographical surface heterogeneity and lateral
471 subsurface transport in a polygonal tundra landscape on soil temperature, soil moisture,
472 and surface energy exchanges. Starting from the climate-scale land model ALMv0, we
473 incorporated in ALMv0-3D numerical representations of subsurface water and energy
474 lateral transport that are solved using PETSc. A simple method for redistributing incoming
475 snow along the microtopographic transect was also integrated in the model.



476 Over the observational record, ALMv0-3D with snow redistribution and lateral heat
477 and hydrological fluxes accurately predicted snow depth and soil temperature vertical
478 profiles in the polygon rims and centers (overall bias, RMSE, and R^2 of 0.59°C, 1.82°C and
479 0.99, respectively). In the rims, the transition to thawed soil in spring, summer
480 temperature dynamics, and minimum temperatures during the winter were all accurately
481 predicted. In the centers, a $\sim 2^\circ\text{C}$ warm bias in April in the 75-100 cm soil layer was
482 predicted, although this bias disappeared during snowmelt.

483 The spatial heterogeneity of snow depth during the winter due to snow
484 redistribution generated surface soil temperature heterogeneity that propagated into the
485 soil over time. The temporal and spatial variation of snow depth was affected by snow
486 redistribution, but not by lateral thermal and hydrologic transport. Both snow
487 redistribution and lateral thermal fluxes affected spatial variability of soil temperatures.
488 Energy dissipation in the lateral direction reduced the depth to which soil temperature
489 variance penetrated. Snow redistribution led to ~ 10 cm shallower active layer depths
490 under the polygon rims because of the residual effect of reduced insulation during the
491 winter. In contrast, snow redistribution led to ~ 5 cm deeper active layers under the
492 polygon centers. The effect of lateral energy fluxes on active layer depths was ~ 3 cm.
493 Compared to 1D physics, the 2D subsurface physics led to lower (higher) soil temperatures
494 with depth and time in the polygon rims (centers). The larger than 1°C wintertime spatial
495 temperature variability down to ~ 2 m depth in rims and centers indicates the uncertainty
496 associated with considering rims and centers as separate 1D columns. During the summer,
497 polygon center temperatures were relatively more vertically homogeneous than
498 temperatures in the rims.

499 The monthly- and spatial-mean predicted latent and sensible heat fluxes were
500 unaffected by snow redistribution and lateral heat and hydrological fluxes. However, snow
501 redistribution led to spatial heterogeneity in surface energy fluxes and soil moisture during
502 the summer. Excluding lateral subsurface hydrologic and thermal processes led to an over
503 prediction of spatial variability in soil moisture and soil temperature because subsurface
504 gradients were artificially prevented from laterally dissipating over time. Snow
505 redistribution effects on soil moisture heterogeneity were larger than those associated
506 with lateral thermal fluxes.



507 Overall, our analysis demonstrates the potential and value of explicitly representing
508 snow redistribution and lateral subsurface hydrologic and thermal dynamics in polygonal
509 ground systems and quantifies the effects of these processes on the resulting system states
510 and surface energy exchanges with the atmosphere. The integration of 3D subsurface
511 processes in the ACME Land Model also allows for a wide range of analyses heretofore
512 impossible in an Earth System Model context.
513



514 **5 Tables**

515 **Table 1. Bias, root mean square error (RMSE), and correlation (R^2) between modeled and**
 516 **observed snow depth at polygon center, rim and difference between center and rim for**
 517 **2013 for three cases: Snow redistribution (SR) off and 1D physics, SR on and 1D physics,**
 518 **and SR on and 2D physics.**

	SR=Off, Physics=1D			SR=On, Physics=1D			SR=On, Physics=2D		
	Center	Rim	Center- Rim	Center	Rim	Center- Rim	Center	Rim	Center- Rim
Bias	-0.08	0.02	-0.1	-0.04	-0.03	-0.02	-0.04	-0.03	-0.02
RMSE	0.12	0.04	0.12	0.08	0.04	0.05	0.08	0.04	0.05
R^2	0.86	0.92	0.03	0.78	0.85	0.73	0.79	0.85	0.73

519

520



521 **Table 2 Bias, root mean square error (RMSE) and correlation (R^2) between modeled and**
 522 **observed soil temperature at polygon center and rim at multiple soil depth for 2013 for**
 523 **three cases: Snow redistribution (SR) off and 1D physics, SR on and 1D physics, and SR on**
 524 **and 2D physics.**

Bias						
	SR=Off, Physics=1D		SR=On, Physics=2D		SR=On, Physics=2D	
Depth [m]	Center	Rim	Center	Rim	Center	Rim
0.00 - 0.20	0.86	-1.73	-0.19	1.00	0.52	0.71
0.20 - 0.50	0.68	-1.52	-0.46	0.98	0.35	0.62
0.50 - 0.75	0.53	-1.49	-0.64	0.94	0.21	0.53
0.75 - 1.00	0.49	-1.44	-0.67	-0.97	0.22	0.49
Average across four depths	0.64	-1.54	-0.49	0.97	0.33	0.59

525

RMSE						
	SR=Off, Physics=1D		SR=On, Physics=2D		SR=On, Physics=2D	
Depth [m]	Center	Rim	Center	Rim	Center	Rim
0.00 - 0.20	2.11	3.39	2.20	2.94	1.90	2.66
0.20 - 0.50	1.49	2.73	1.39	1.86	1.12	1.57
0.50 - 0.75	1.60	2.42	1.22	1.96	1.14	1.60
0.75 - 1.00	1.50	2.15	1.12	1.87	1.09	1.44
Average across four depths	1.67	2.67	1.44	2.16	1.31	1.82

526

R^2						
	SR=Off, Physics=1D		SR=On, Physics=2D		SR=On, Physics=2D	
Depth [m]	Center	Rim	Center	Rim	Center	Rim
0.00 - 0.20	0.98	0.95	0.97	0.97	0.98	0.97



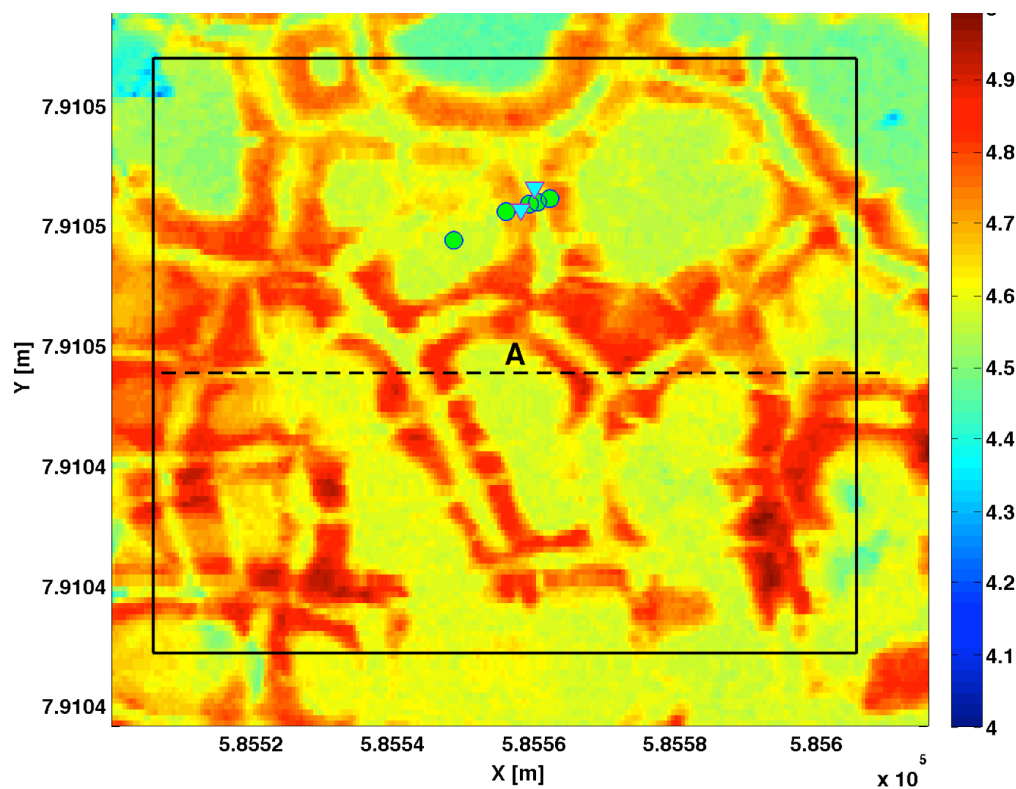
0.20 - 0.50	0.99	0.96	0.98	0.99	0.99	0.99
0.50 - 0.75	0.99	0.97	0.99	0.99	1.00	0.99
0.75 - 1.00	0.99	0.97	0.99	0.99	1.00	0.99
Average across four depths	0.99	0.96	0.98	0.99	0.99	0.99

527



528

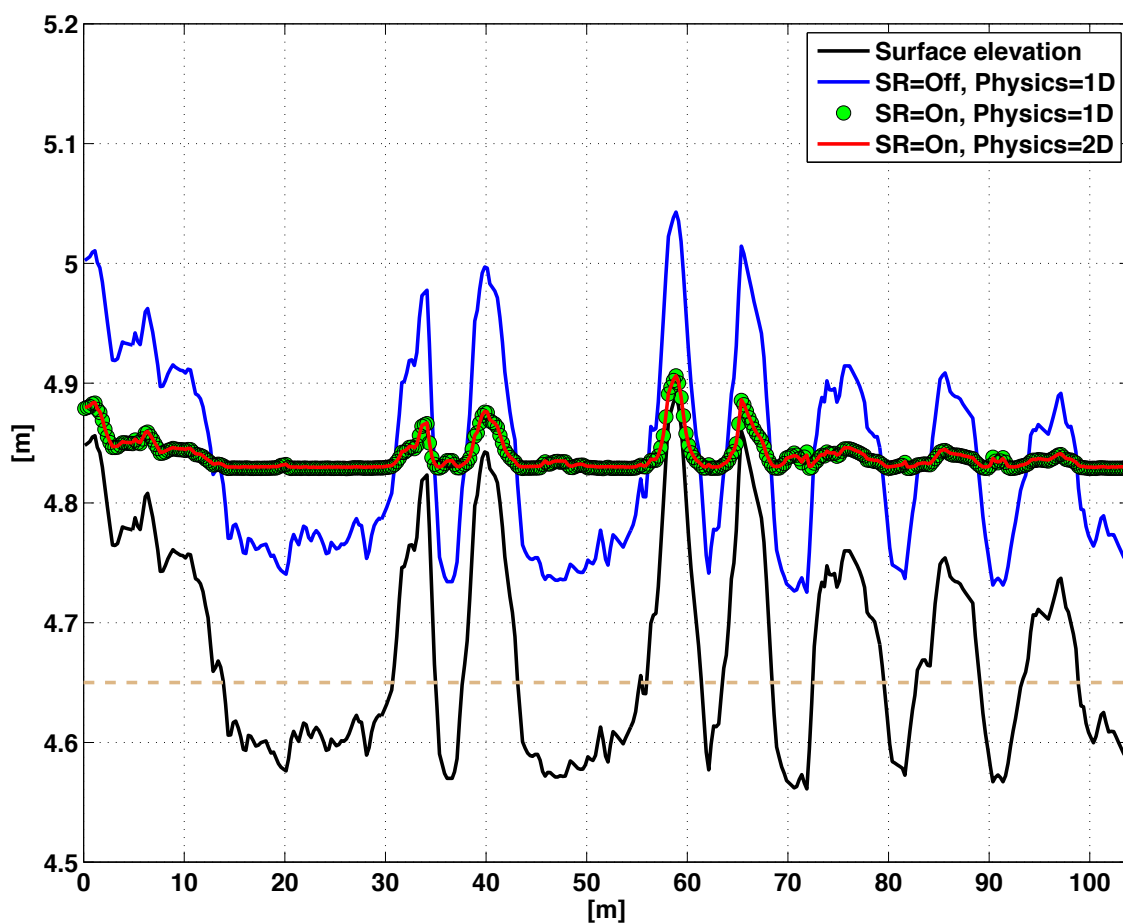
529 6 Figures



530

531 **Figure 1** The NGEE-Arctic study area A, which characterized as a low-centered polygon
532 field. Dotted line indicate the transect along which simulation in this paper are performed
533 to demonstrate the effects of snow redistribution on soil temperature. The locations where
534 snow and temperature sensors are installed within the study site are denoted by triangle
535 and circle, respectively.

536



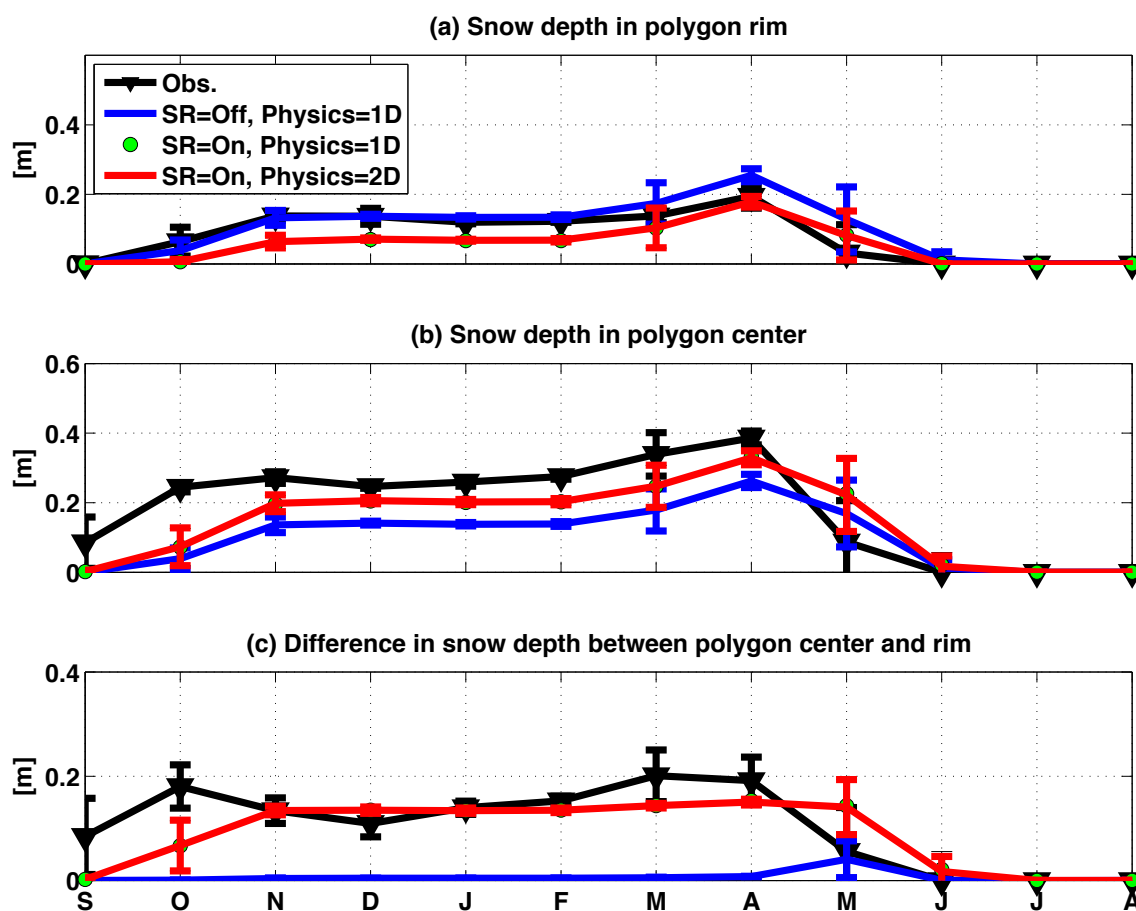
537

538 **Figure 2. Simulated average winter snow surface elevation across the transect for three**
539 **scenarios: (1) snow redistribution (SR) turned off and 1D subsurface physics, (2) snow**
540 **redistribution turned on and 1D subsurface physics, and (3) snow redistribution turned on**
541 **and 2D subsurface physics. Surface elevation of the transect is shown by solid black line.**
542 **The dashed line indicates the boundary for comparison to observations in relatively lower**
543 **(centers) and relatively higher (rims) topographical positions.**



544

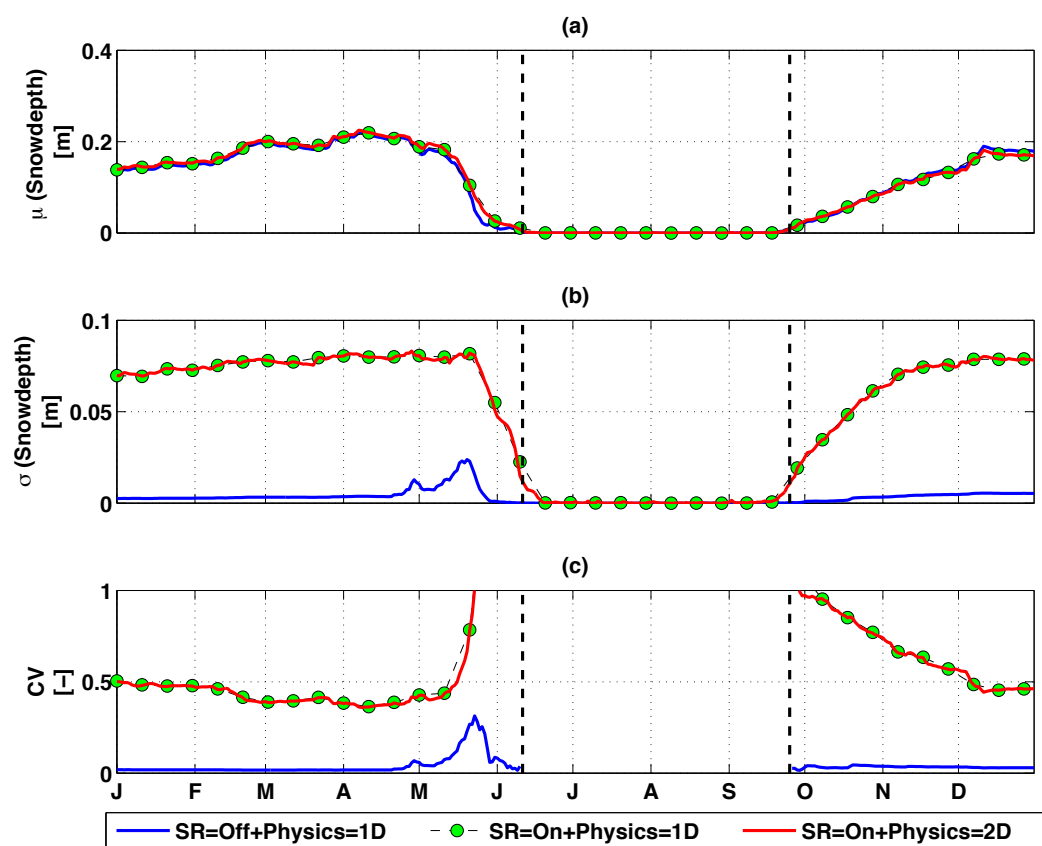
545



546

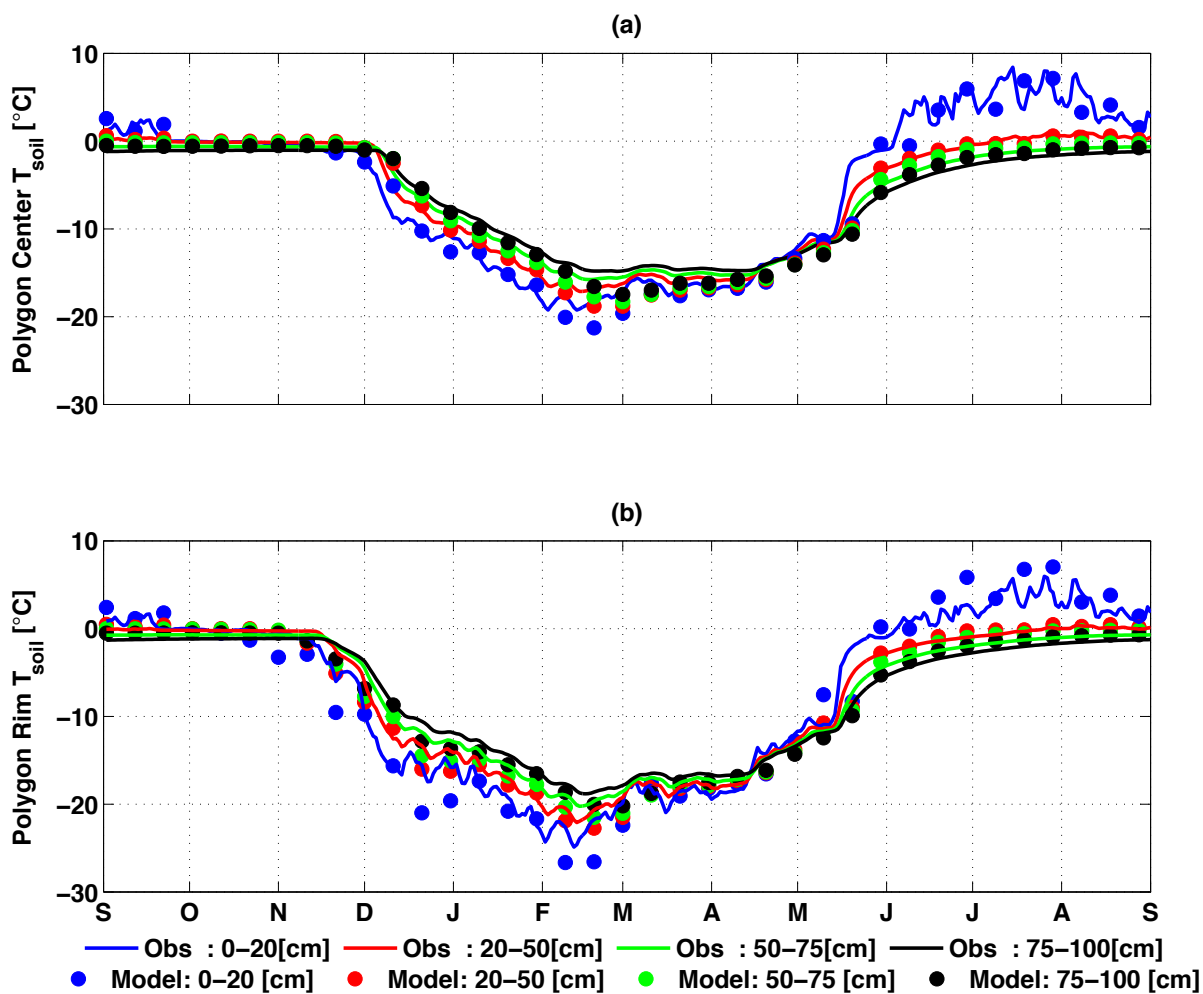
547

548 **Figure 3** Monthly-mean comparison of observation and simulated snow depth (a) in
549 polygon rim, (b) in polygon center; (c) difference between polygon center and rim for 2013.



550

551 **Figure 4. Mean, standard deviation and coefficient of variation of simulated snow**
552 **depth across the entire domain for 1D and 2D subsurface physics.**

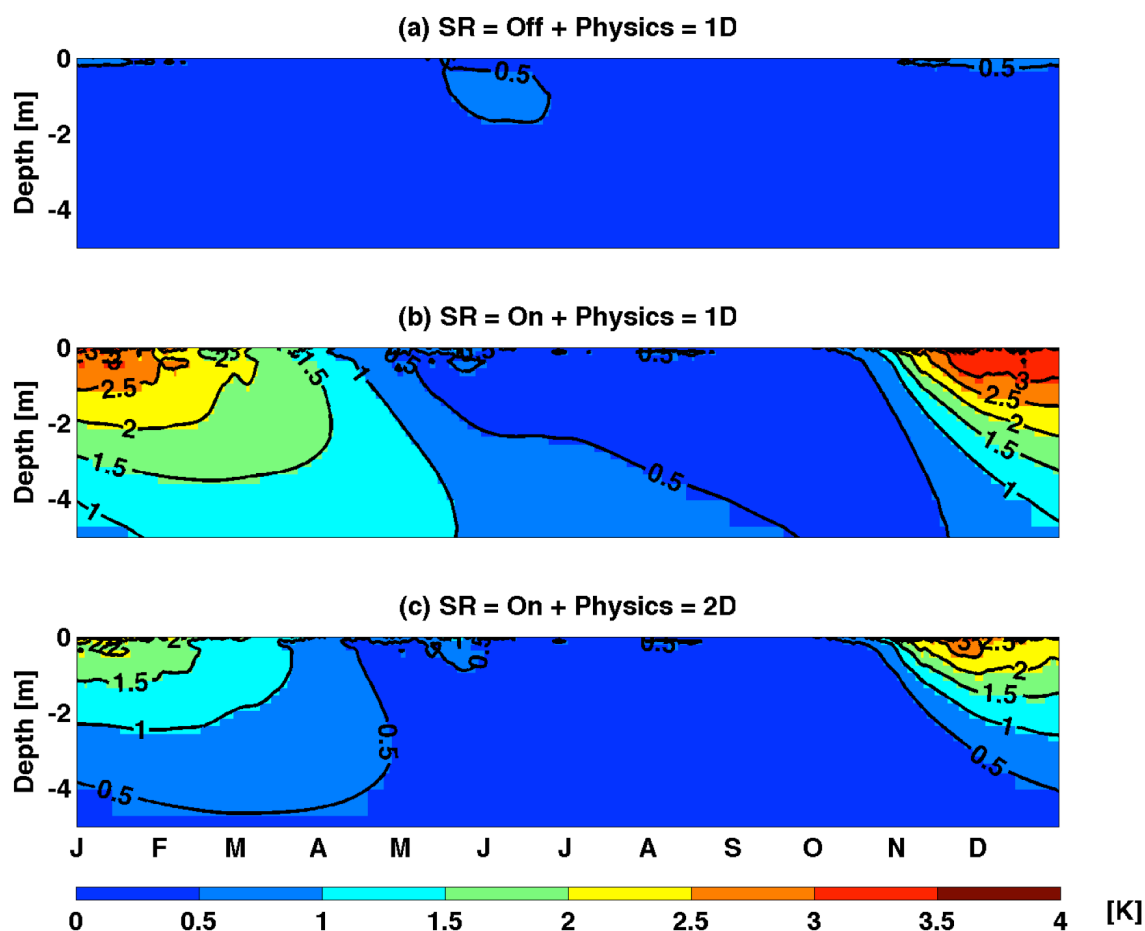


553

554 **Figure 5 Comparison of soil temperature observations and predictions in polygon centers**
555 **(a) and rims (b). Simulation was performed with snow redistribution on and 2D subsurface**
556 **physics, between September 2012 and September 2013. Simulation results are shown at an**
557 **interval of 10 days, while observations are shown at daily interval**

558

559

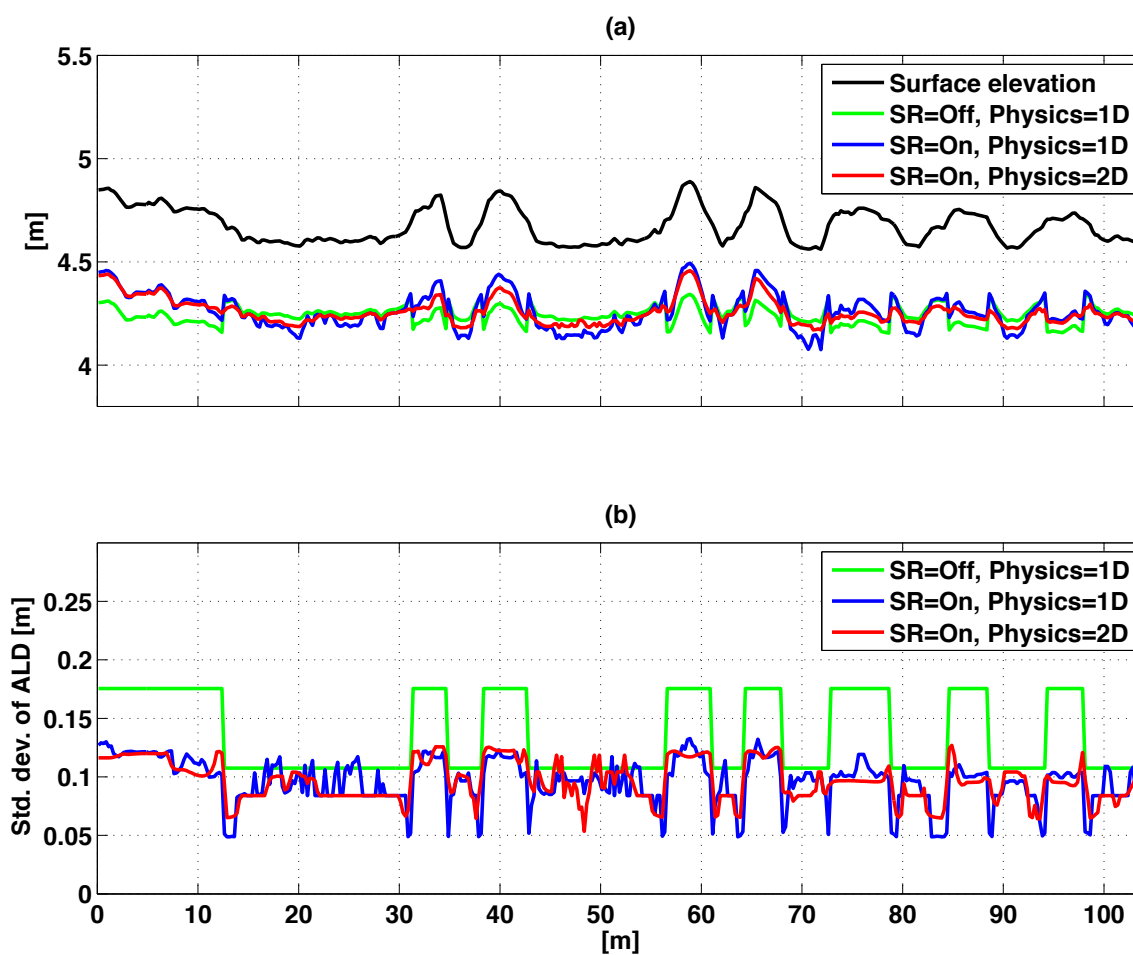


560

561 **Figure 6 Simulated daily spatial standard deviation averaged across 10-year of near**
562 **surface soil temperature for simulation performed with snow redistribution turned off and**
563 **1D subsurface physics (top panel); snow redistribution turned on and 1D subsurface**
564 **physics (middle panel); and snow redistribution turned on and 2D subsurface physics**
565 **(bottom panel).**

566

567



568

569

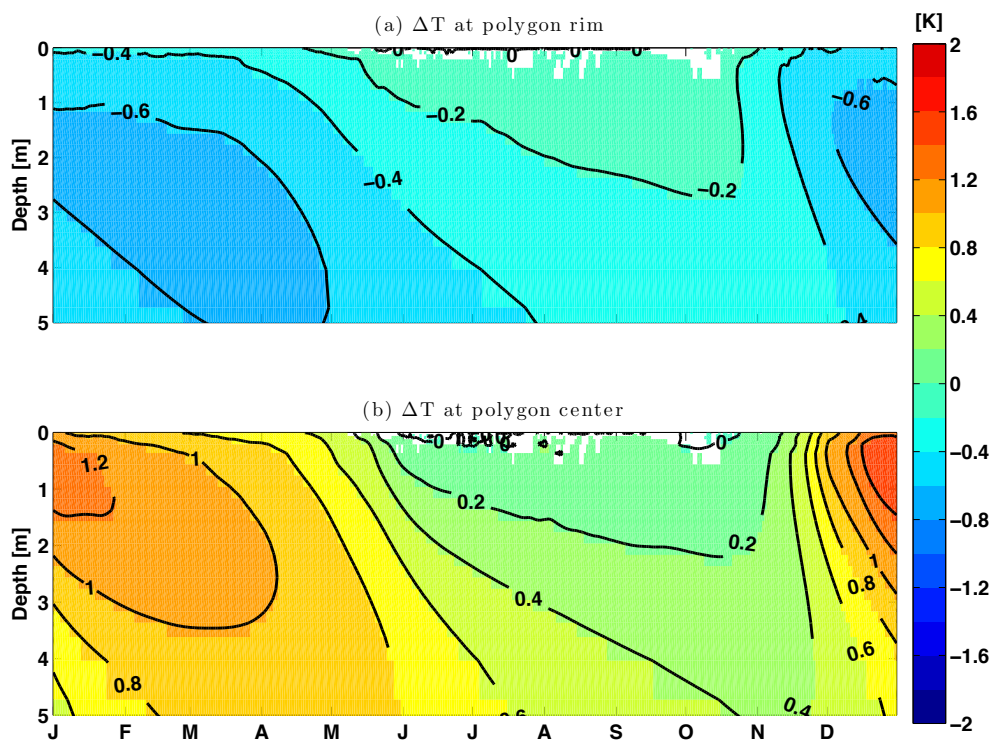
570 **Figure 7** Temporal mean of the bottom of the active layer (top panel) and standard
571 deviation of the active layer depth (bottom panel) over the 10-year period across the
572 modeling domain.

573



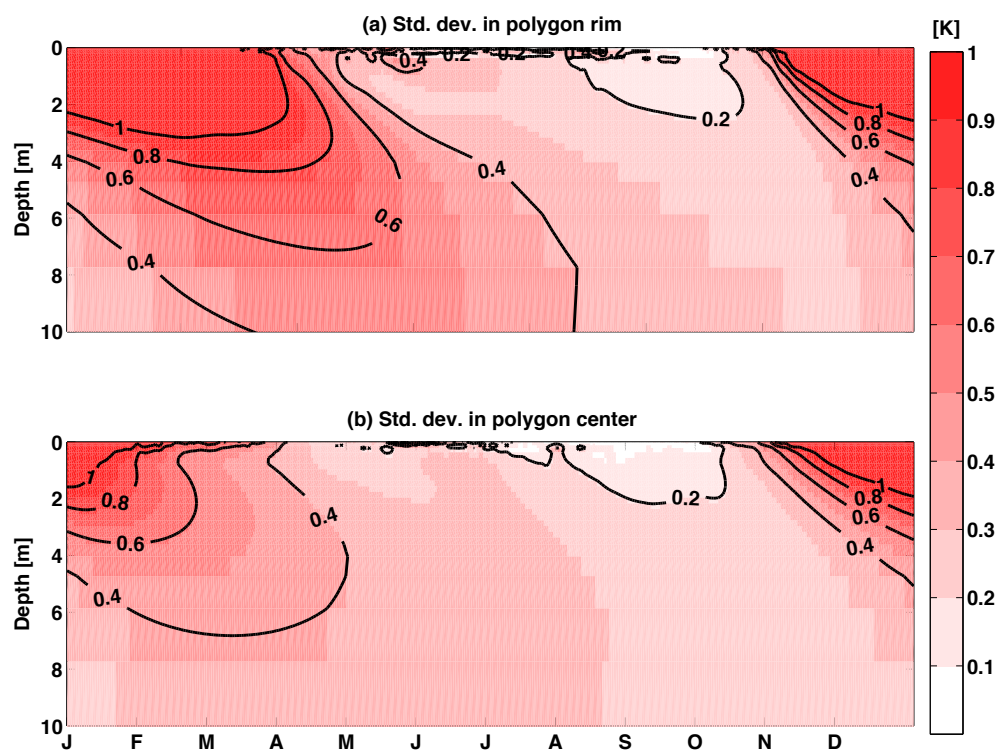
574

575



576

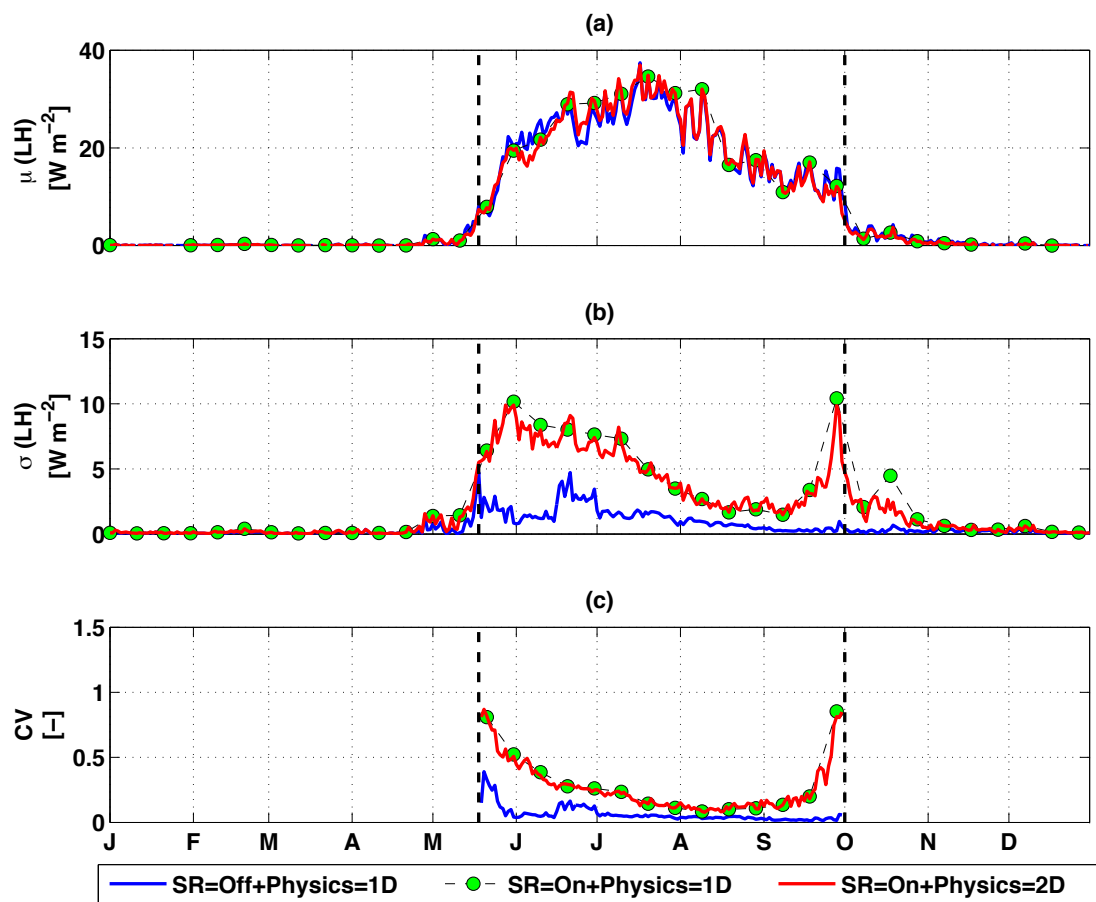
577 **Figure 8 Time series of spatial mean soil temperature differences between “SR=On +**
578 **Physics=1D” and “SR=On + Physics=2D” at polygon rim (top panel) and polygon center**
579 **(bottom panel).**



580

581 **Figure 9 Time series of soil temperature spatial standard deviation for “SR=On +**

582 **Physics=2D” at polygon rim (top panel) and polygon center (bottom panel).**



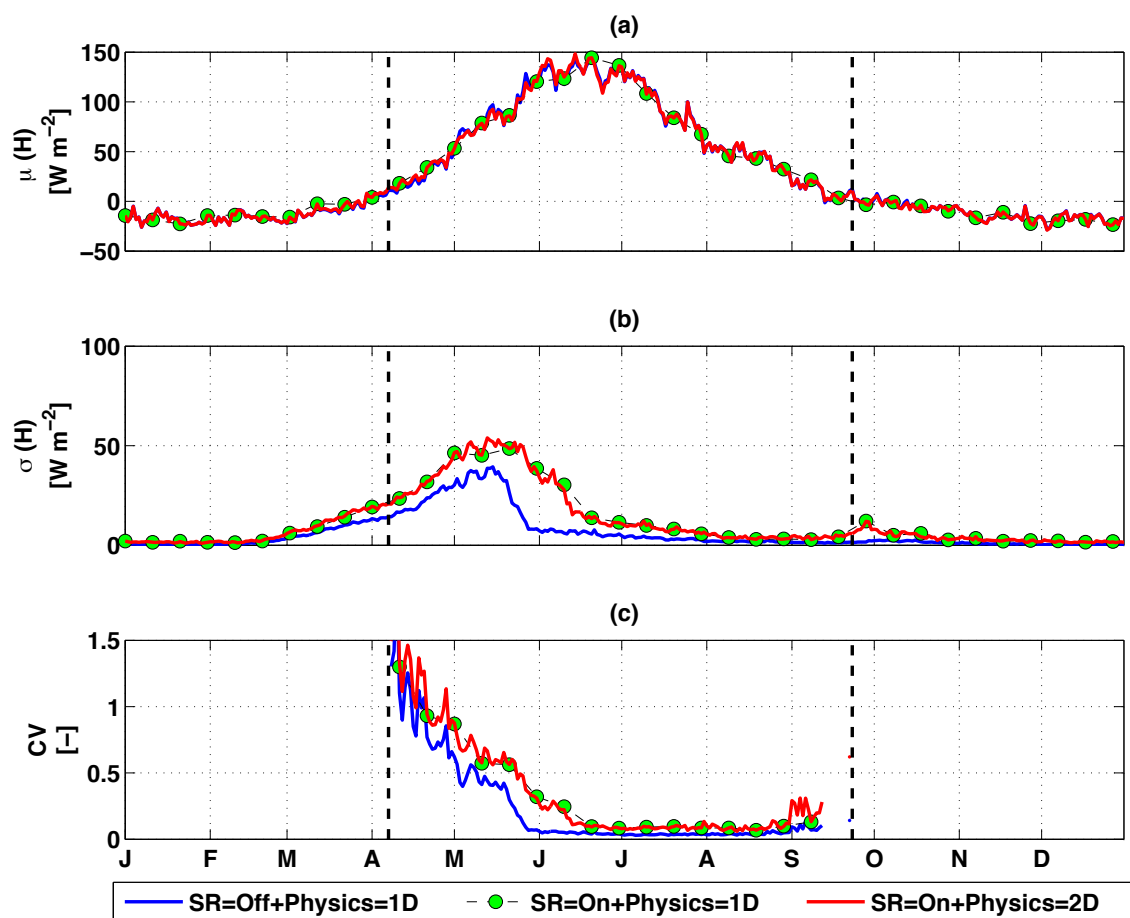
583

584

585 **Figure 10. Latent heat flux inter-annual (a) mean, (b) standard deviation, and (c)**

586 **coefficient of variation across the site A transect.**

587

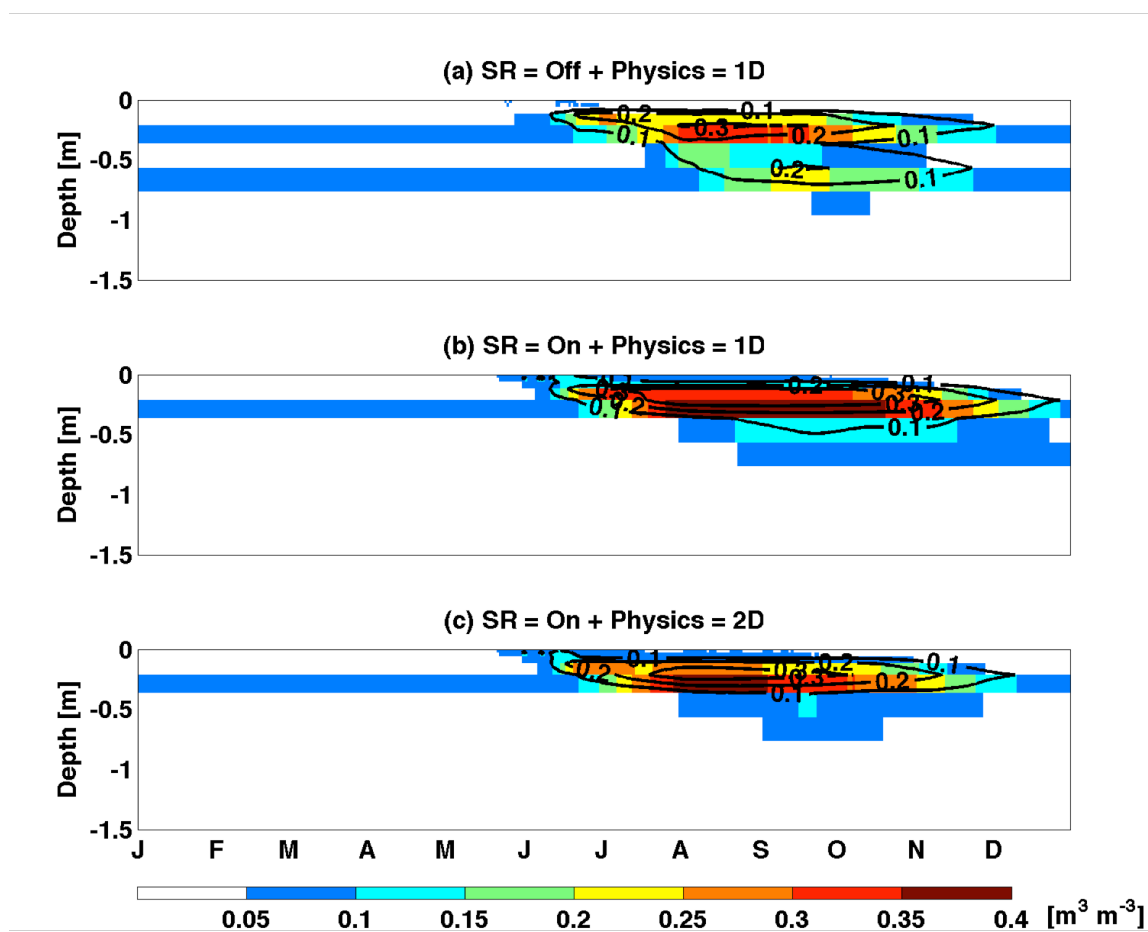


588

589

590 **Figure 11.** Same as Figure 10 except for sensible heat flux.

591



592

593 Figure 12. Same as Figure 6 except for liquid saturation.



594 **Acknowledgements.**

595 This research was supported by the Director, Office of Science, Office of Biological and
596 Environmental Research of the US Department of Energy under Contract No. DE-AC02-
597 05CH11231 as part of the NGEE-Arctic and Accelerated Climate Modeling for Energy (ACME)
598 programs.



599 References

- 600 Anderson, E. A.: A point energy and mass balance model of a snow cover, National Weather
601 Service, Silver Spring, MD, 1976.
- 602 Balay, S., Abhyankar, S., Adams, M. F., Brown, J., Brune, P., Buschelman, K., Dalcin, L.,
603 Eijkhout, V., Gropp, W. D., Kaushik, D., Knepley, M. G., McInnes, L. C., Rupp, K., Smith, B.
604 F., Zampini, S., Zhang, H., and Zhang, H.: PETSc Users Manual, Argonne National Laboratory,
605 2016.
- 606 Barber, V. A., Juday, G. P., and Finney, B. P.: Reduced growth of Alaskan white spruce in the
607 twentieth century from temperature-induced drought stress, *Nature*, 405, 668-673, 2000.
- 608 Bartelt, P. and Lehning, M.: A physical SNOWPACK model for the Swiss avalanche warning:
609 Part I: numerical model, *Cold Regions Science and Technology*, 35, 123-145, 2002.
- 610 Borner, A. P., Kielland, K., and Walker, M. D.: Effects of Simulated Climate Change on Plant
611 Phenology and Nitrogen Mineralization in Alaskan Arctic Tundra, *Arctic, Antarctic, and Alpine*
612 *Research*, 40, 27-38, 2008.
- 613 Callaghan, T., Johansson, M., Brown, R., Groisman, P., Labba, N., Radionov, V., Barry, R.,
614 Bulygina, O., Essery, R. H., Frolov, D. M., Golubev, V., Grenfell, T., Petrushina, M., Razuvaev,
615 V., Robinson, D., Romanov, P., Shindell, D., Shmakin, A., Sokratov, S., Warren, S., and Yang,
616 D.: The Changing Face of Arctic Snow Cover: A Synthesis of Observed and Projected Changes,
617 *AMBIO*, 40, 17-31, 2011a.
- 618 Callaghan, T., Johansson, M., Brown, R., Groisman, P., Labba, N., Radionov, V., Bradley, R.,
619 Blangy, S., Bulygina, O., Christensen, T., Colman, J., Essery, R. H., Forbes, B., Forchhammer,
620 M., Golubev, V., Honrath, R., Juday, G., Meshcherskaya, A., Phoenix, G., Pomeroy, J., Rautio,
621 A., Robinson, D., Schmidt, N., Serreze, M., Shevchenko, V., Shiklomanov, A., Shmakin, A.,
622 Sköld, P., Sturm, M., Woo, M.-k., and Wood, E.: Multiple Effects of Changes in Arctic Snow
623 Cover, *AMBIO*, 40, 32-45, 2011b.
- 624 Chapin, F. S., Shaver, G. R., Giblin, A. E., Nadelhoffer, K. J., and Laundre, J. A.: Responses of
625 Arctic Tundra to Experimental and Observed Changes in Climate, *Ecology*, 76, 694-711, 1995.
- 626 Clark, M. P., Hendrikx, J., Slater, A. G., Kavetski, D., Anderson, B., Cullen, N. J., Kerr, T., Örn
627 Hreinsson, E., and Woods, R. A.: Representing spatial variability of snow water equivalent in
628 hydrologic and land-surface models: A review, *Water Resources Research*, 47, W07539, 2011.



- 629 Cornelissen, J. H. C., Callaghan, T. V., Alatalo, J. M., Michelsen, A., Graglia, E., Hartley, A. E.,
630 Hik, D. S., Hobbie, S. E., Press, M. C., Robinson, C. H., Henry, G. H. R., Shaver, G. R.,
631 Phoenix, G. K., Gwynn Jones, D., Jonasson, S., Chapin, F. S., Molau, U., Neill, C., Lee, J. A.,
632 Melillo, J. M., Sveinbjörnsson, B., and Aerts, R.: Global change and arctic ecosystems: is lichen
633 decline a function of increases in vascular plant biomass?, *Journal of Ecology*, 89, 984-994,
634 2001.
- 635 Cox, P. M., Betts, R. A., Jones, C. D., Spall, S. A., and Totterdell, I. J.: Acceleration of global
636 warming due to carbon-cycle feedbacks in a coupled climate model, *Nature*, 408, 184-187, 2000.
- 637 Dai, Y. and Zeng, Q.: A land surface model (IAP94) for climate studies part I: Formulation and
638 validation in off-line experiments, *Advances in Atmospheric Sciences*, 14, 433-460, 1997.
- 639 Davidson, E. A. and Janssens, I. A.: Temperature sensitivity of soil carbon decomposition and
640 feedbacks to climate change, *Nature*, 440, 165-173, 2006.
- 641 Dufresne, J. L., Fairhead, L., Le Treut, H., Berthelot, M., Bopp, L., Ciais, P., Friedlingstein, P.,
642 and Monfray, P.: On the magnitude of positive feedback between future climate change and the
643 carbon cycle, *Geophysical Research Letters*, 29, 43-41-43-44, 2002.
- 644 Engstrom, R., Hope, A., Kwon, H., Stow, D., and Zamolodchikov, D.: Spatial distribution of
645 near surface soil moisture and its relationship to microtopography in the Alaskan Arctic coastal
646 plain, *Nordic Hydrology*, 36, 219-234, 2005.
- 647 Euskirchen, E. S., McGuire, A. D., Chapin, F. S., Yi, S., and Thompson, C. C.: Changes in
648 vegetation in northern Alaska under scenarios of climate change, 2003–2100: implications for
649 climate feedbacks, *Ecological Applications*, 19, 1022-1043, 2009.
- 650 Euskirchen, E. S., McGuire, A. D., Kicklighter, D. W., Zhuang, Q., Clein, J. S., Dargaville, R. J.,
651 Dye, D. G., Kimball, J. S., McDonald, K. C., Melillo, J. M., Romanovsky, V. E., and Smith, N.
652 V.: Importance of recent shifts in soil thermal dynamics on growing season length, productivity,
653 and carbon sequestration in terrestrial high-latitude ecosystems, *Global Change Biology*, 12,
654 731-750, 2006.
- 655 Frey, S. and Holzmann, H.: A conceptual, distributed snow redistribution model, *Hydrol. Earth
656 Syst. Sci.*, 19, 4517-4530, 2015.
- 657 Friedlingstein, P., Bopp, L., Ciais, P., Dufresne, J.-L., Fairhead, L., LeTreut, H., Monfray, P.,
658 and Orr, J.: Positive feedback between future climate change and the carbon cycle, *Geophysical
659 Research Letters*, 28, 1543-1546, 2001.



- 660 Friedlingstein, P., Cox, P., Betts, R., Bopp, L., von Bloh, W., Brovkin, V., Cadule, P., Doney, S.,
661 Eby, M., Fung, I., Bala, G., John, J., Jones, C., Joos, F., Kato, T., Kawamiya, M., Knorr, W.,
662 Lindsay, K., Matthews, H. D., Raddatz, T., Rayner, P., Reick, C., Roeckner, E., Schnitzler, K.
663 G., Schnur, R., Strassmann, K., Weaver, A. J., Yoshikawa, C., and Zeng, N.: Climate–Carbon
664 Cycle Feedback Analysis: Results from the C4MIP Model Intercomparison, *Journal of Climate*,
665 19, 3337-3353, 2006.
- 666 Fung, I. Y., Doney, S. C., Lindsay, K., and John, J.: Evolution of carbon sinks in a changing
667 climate, *Proceedings of the National Academy of Sciences of the United States of America*, 102,
668 11201-11206, 2005.
- 669 Galen, C. and Stanton, M. L.: Responses of Snowbed Plant Species to Changes in Growing-
670 Season Length, *Ecology*, 76, 1546-1557, 1995.
- 671 Ghimire, B., Riley, W. J., Koven, C. D., Mu, M., and Randerson, J. T.: Representing leaf and
672 root physiological traits in CLM improves global carbon and nitrogen cycling predictions,
673 *Journal of Advances in Modeling Earth Systems*, 8, 598-613, 2016.
- 674 Govindasamy, B., Thompson, S., Mirin, A., Wickett, M., Caldeira, K., and Delire, C.: Increase
675 of carbon cycle feedback with climate sensitivity: results from a coupled climate and carbon
676 cycle model, *Tellus B*, 57, 2011.
- 677 Groendahl, L., Friborg, T., and Soegaard, H.: Temperature and snow-melt controls on
678 interannual variability in carbon exchange in the high Arctic, *Theoretical and Applied*
679 *Climatology*, 88, 111-125, 2007.
- 680 Grogan, P. and Chapin Iii, F. S.: Arctic Soil Respiration: Effects of Climate and Vegetation
681 Depend on Season, *Ecosystems*, 2, 451-459, 1999.
- 682 Hartman, M. D., Baron, J. S., Lammers, R. B., Cline, D. W., Band, L. E., Liston, G. E., and
683 Tague, C.: Simulations of snow distribution and hydrology in a mountain basin, *Water Resources*
684 *Research*, 35, 1587-1603, 1999.
- 685 Helfricht, K., Schöber, J., Seiser, B., Fischer, A., Stötter, J., and Kuhn, M.: Snow accumulation
686 of a high alpine catchment derived from LiDAR measurements, *Adv. Geosci.*, 32, 31-39, 2012.
- 687 Hinkel, K. M., Eisner, W. R., Bockheim, J. G., Nelson, F. E., Peterson, K. M., and Dai, X.:
688 Spatial Extent, Age, and Carbon Stocks in Drained Thaw Lake Basins on the Barrow Peninsula,
689 *Alaska, Arctic, Antarctic and Alpine Research*, 35, 291-300, 2003.



- 690 Hinkel, K. M., Frohn, R. C., Nelson, F. E., Eisner, W. R., and Beck, R. A.: Morphometric and
691 spatial analysis of thaw lakes and drained thaw lake basins in the western Arctic Coastal Plain,
692 Alaska, *Permafrost and Periglacial Processes*, 16, 327-341, 2005.
- 693 Hinzman, L. D. and Kane, D. L.: Potential repsonse of an Arctic watershed during a period of
694 global warming, *Journal of Geophysical Research: Atmospheres*, 97, 2811-2820, 1992.
- 695 Hobbie, S. E.: Temperature and Plant Species Control Over Litter Decomposition in Alaskan
696 Tundra, *Ecological Monographs*, 66, 503-522, 1996.
- 697 Hobbie, S. E. and Chapin, F. S.: THE RESPONSE OF TUNDRA PLANT BIOMASS,
698 ABOVEGROUND PRODUCTION, NITROGEN, AND CO₂ FLUX TO EXPERIMENTAL
699 WARMING, *Ecology*, 79, 1526-1544, 1998.
- 700 Holland, M. M. and Bitz, C. M.: Polar amplification of climate change in coupled models,
701 *Climate Dynamics*, 21, 221-232, 2003.
- 702 Hollister, R. D., Webber, P. J., and Bay, C.: PLANT RESPONSE TO TEMPERATURE IN
703 NORTHERN ALASKA: IMPLICATIONS FOR PREDICTING VEGETATION CHANGE,
704 *Ecology*, 86, 1562-1570, 2005.
- 705 Jiang, D., Zhang, Y., and Lang, X.: Vegetation feedback under future global warming,
706 *Theoretical and Applied Climatology*, 106, 211-227, 2011.
- 707 Jones, C. D., Cox, P. M., Essery, R. L. H., Roberts, D. L., and Woodage, M. J.: Strong carbon
708 cycle feedbacks in a climate model with interactive CO₂ and sulphate aerosols, *Geophysical
709 Research Letters*, 30, 1479, 2003.
- 710 Jones, H. G.: The ecology of snow-covered systems: a brief overview of nutrient cycling and life
711 in the cold, *Hydrological Processes*, 13, 2135-2147, 1999.
- 712 Jordan, R. E.: One-dimensional temperature model for a snow cover : technical documentation
713 for SNTHERM.89, Cold Regions Research and Engineering Laboratory (U.S.) Engineer
714 Research and Development Center (U.S.), 1991.
- 715 Jorgenson, M. T., Shur, Y. L., and Pullman, E. R.: Abrupt increase in permafrost degradation in
716 Arctic Alaska, *Geophysical Research Letters*, 33, L02503, 2006.
- 717 Koven, C. D., Lawrence, D. M., and Riley, W. J.: Permafrost carbon–climate feedback is
718 sensitive to deep soil carbon decomposability but not deep soil nitrogen dynamics, *Proceedings
719 of the National Academy of Sciences*, 112, 3752-3757, 2015.



- 720 Koven, C. D., Riley, W. J., Subin, Z. M., Tang, J. Y., Torn, M. S., Collins, W. D., Bonan, G. B.,
721 Lawrence, D. M., and Swenson, S. C.: The effect of vertically resolved soil biogeochemistry and
722 alternate soil C and N models on C dynamics of CLM4, *Biogeosciences*, 10, 7109-7131, 2013.
- 723 Koven, C. D., Ringeval, B., Friedlingstein, P., Ciais, P., Cadule, P., Khvorostyanov, D., Krinner,
724 G., and Tarnocai, C.: Permafrost carbon-climate feedbacks accelerate global warming,
725 *Proceedings of the National Academy of Sciences*, 108, 14769-14774, 2011.
- 726 Lawrence, D. M. and Swenson, S. C.: Permafrost response to increasing Arctic shrub abundance
727 depends on the relative influence of shrubs on local soil cooling versus large-scale climate
728 warming, *Environmental Research Letters*, 6, 045504, 2011.
- 729 Liston, G. E. and Elder, K.: A Distributed Snow-Evolution Modeling System (SnowModel),
730 *Journal of Hydrometeorology*, 7, 1259-1276, 2006.
- 731 Liston, G. E., Haehnel, R. B., Sturm, M., Hiemstra, C. A., Berezovskaya, S., and Tabler, R. D.:
732 Instruments and Methods
733 `xmlns="http://pub2web.metastore.ingenta.com/ns/">
`
734 Simulating complex snow distributions in windy environments using SnowTran-3D, *Journal of*
735 *Glaciology*, 53, 241-256, 2007.
- 736 Lopez-Moreno, J. I., Fassnacht, S. R., Begueria, S., and Latron, J.: Variability of snow depth at
737 the plot scale: implications for mean depth estimation and sampling strategies, 2011. 2011.
- 738 López-Moreno, J. I., Revuelto, J., Fassnacht, S. R., Azorín-Molina, C., Vicente-Serrano, S. M.,
739 Morán-Tejeda, E., and Sexstone, G. A.: Snowpack variability across various spatio-temporal
740 resolutions, *Hydrological Processes*, doi: 10.1002/hyp.10245, 2014. n/a-n/a, 2014.
- 741 Luce, C. H., Tarboton, D. G., and Cooley, K. R.: The influence of the spatial distribution of snow
742 on basin-averaged snowmelt, *Hydrological Processes*, 12, 1671-1683, 1998.
- 743 Lundquist, J. D. and Dettinger, M. D.: How snowpack heterogeneity affects diurnal streamflow
744 timing, *Water Resources Research*, 41, W05007, 2005.
- 745 Mack, M. C., Schuur, E. A. G., Bret-Harte, M. S., Shaver, G. R., and Chapin, F. S.: Ecosystem
746 carbon storage in arctic tundra reduced by long-term nutrient fertilization, *Nature*, 431, 440-443,
747 2004.
- 748 Matthews, H. D., Eby, M., Ewen, T., Friedlingstein, P., and Hawkins, B. J.: What determines the
749 magnitude of carbon cycle-climate feedbacks?, *Global Biogeochemical Cycles*, 21, n/a-n/a,
2007a.



- 750 Matthews, H. D., Eby, M., Ewen, T., Friedlingstein, P., and Hawkins, B. J.: What determines the
751 magnitude of carbon cycle-climate feedbacks?, *Global Biogeochemical Cycles*, 21, GB2012,
752 2007b.
- 753 Matthews, H. D., Weaver, A. J., and Meissner, K. J.: Terrestrial Carbon Cycle Dynamics under
754 Recent and Future Climate Change, *Journal of Climate*, 18, 1609-1628, 2005.
- 755 McFadden, J. P., Chapin, F. S., and Hollinger, D. Y.: Subgrid-scale variability in the surface
756 energy balance of arctic tundra, *Journal of Geophysical Research: Atmospheres*, 103, 28947-
757 28961, 1998.
- 758 McGuire, A. D., Clein, J. S., Melillo, J. M., Kicklighter, D. W., Meier, R. A., Vorosmarty, C. J.,
759 and Serreze, M. C.: Modelling carbon responses of tundra ecosystems to historical and projected
760 climate: sensitivity of pan-Arctic carbon storage to temporal and spatial variation in climate,
761 *Global Change Biology*, 6, 141-159, 2000.
- 762 Mefford, T. K., Bieniulis, M., Halter, B., and Peterson, J.: *Meteorological Measurements*, 17 pp.,
763 1996.
- 764 Miller, P. C., Stoner, W. A., and Tieszen, L. L.: A Model of Stand Photosynthesis for the Wet
765 Meadow Tundra at Barrow, Alaska, *Ecology*, 57, 411-430, 1976.
- 766 Morgner, E., Elberling, B., Strebel, D., and Cooper, E. J.: The importance of winter in annual
767 ecosystem respiration in the High Arctic: effects of snow depth in two vegetation types, *Polar*
768 *Research*, 29, 58-74, 2010.
- 769 Nobrega, S. and Grogan, P.: Deeper Snow Enhances Winter Respiration from Both Plant-
770 associated and Bulk Soil Carbon Pools in Birch Hummock Tundra, *Ecosystems*, 10, 419-431,
771 2007.
- 772 Oberbauer, S. F., Tenhunen, J. D., and Reynolds, J. F.: Environmental Effects on CO₂ Efflux
773 from Water Track and Tussock Tundra in Arctic Alaska, U.S.A, *Arctic and Alpine Research*, 23,
774 162-169, 1991.
- 775 Oechel, W. C., Hastings, S. J., Vourlitis, G., Jenkins, M., Riechers, G., and Grulke, N.: Recent
776 change of Arctic tundra ecosystems from a net carbon dioxide sink to a source, *Nature*, 361, 520-
777 523, 1993.
- 778 Oleson, K. W., D.M. Lawrence, G.B. Bonan, B. Drewniak, M. Huang, C.D. Koven, S. Levis, F.
779 Li, W.J. Riley, Z.M. Subin, S.C. Swenson, P.E. Thornton, A. Bozbiyik, R. Fisher, E. Kluzek, J.-
780 F. Lamarque, P.J. Lawrence, L.R. Leung, W. Lipscomb, S. Muszala, D.M. Ricciuto, W. Sacks,



- 781 Y. Sun, J. Tang, Z.-L. Yang: Technical Description of version 4.5 of the Community Land
782 Model (CLM), National Center for Atmospheric Research, Boulder, CO, 422 pp., 2013a.
- 783 Oleson, K. W., D.M. Lawrence, G.B. Bonan, B. Drewniak, M. Huang, C.D. Koven, S. Levis, F.
784 Li, W.J. Riley, Z.M. Subin, S.C. Swenson, P.E. Thornton, A. Bozbiyik, R. Fisher, E. Kluzek, J-
785 F. Lamarque, P.J. Lawrence, L.R. Leung, W. Lipscomb, S. Muszala, D.M. Ricciuto, W. Sacks,
786 Y. Sun, J. Tang, Z.-L. Yang: Technical Description of version 4.5 of the Community Land
787 Model (CLM), National Center for Atmospheric Research, Boulder, CO, 2013b.
- 788 Randerson, J. T., Lindsay, K., Munoz, E., Fu, W., Moore, J. K., Hoffman, F. M., Mahowald, N.
789 M., and Doney, S. C.: Multicentury changes in ocean and land contributions to the climate-
790 carbon feedback, *Global Biogeochemical Cycles*, 29, 744-759, 2015.
- 791 Rogers, M. C., Sullivan, P. F., and Welker, J. M.: Evidence of Nonlinearity in the Response of
792 Net Ecosystem CO₂ Exchange to Increasing Levels of Winter Snow Depth in the High Arctic of
793 Northwest Greenland, *Arctic, Antarctic, and Alpine Research*, 43, 95-106, 2011.
- 794 Rohrbough, J. A., Davis, D. R., and Bales, R. C.: Spatial variability of snow chemistry in an
795 alpine snowpack, southern Wyoming, *Water Resources Research*, 39, 1190, 2003.
- 796 Schaefer, K., Zhang, T., Bruhwiler, L., and Barrett, A. P.: Amount and timing of permafrost
797 carbon release in response to climate warming, *Tellus B*, 63, 165-180, 2011.
- 798 Schimel, J. P., Bilbrough, C., and Welker, J. M.: Increased snow depth affects microbial activity
799 and nitrogen mineralization in two Arctic tundra communities, *Soil Biology and Biochemistry*,
800 36, 217-227, 2004.
- 801 Schimel, J. P., Kielland, K., and Chapin, F. S., III: Nutrient Availability and Uptake by Tundra
802 Plants. In: *Landscape Function and Disturbance in Arctic Tundra*, Reynolds, J. and Tenhunen, J.
803 (Eds.), *Ecological Studies*, Springer Berlin Heidelberg, 1996.
- 804 Schuur, E. A. G. and Abbott, B.: Climate change: High risk of permafrost thaw, *Nature*, 480, 32-
805 33, 2011.
- 806 Schuur, E. A. G., Bockheim, J., Canadell, J. G., Euskirchen, E., Field, C. B., Goryachkin, S. V.,
807 Hagemann, S., Kuhry, P., Lafleur, P. M., Lee, H., Mazhitova, G., Nelson, F. E., Rinke, A.,
808 Romanovsky, V. E., Shiklomanov, N., Tarnocai, C., Venevsky, S., Vogel, J. G., and Zimov, S.
809 A.: Vulnerability of Permafrost Carbon to Climate Change: Implications for the Global Carbon
810 Cycle, *BioScience*, 58, 701-714, 2008.



- 811 Seppala, M., Gray, J., and Ricard, J.: Development of low-centred ice-wedge polygons in the
812 northernmost Ungava Peninsul, Québec, Canada, *Boreas*, 20, 259-285, 1991.
- 813 Sexstone, G. A. and Fassnacht, S. R.: What drives basin scale spatial variability of snowpack
814 properties in northern Colorado?, *The Cryosphere*, 8, 329-344, 2014.
- 815 Shaver, G. and Chapin III, F.: Effect of fertilizer on production and biomass of tussock tundra,
816 Alaska, USA, *Arctic and Alpine Research*, 1986. 261-268, 1986.
- 817 Shaver, G. R. and Chapin, F. S.: Production: Biomass Relationships and Element Cycling in
818 Contrasting Arctic Vegetation Types, *Ecological Monographs*, 61, 1-31, 1991.
- 819 Sitch, S., Huntingford, C., Gedney, N., Levy, P. E., Lomas, M., Piao, S. L., Betts, R., Ciais, P.,
820 Cox, P., Friedlingstein, P., Jones, C. D., Prentice, I. C., and Woodward, F. I.: Evaluation of the
821 terrestrial carbon cycle, future plant geography and climate-carbon cycle feedbacks using five
822 Dynamic Global Vegetation Models (DGVMs), *Global Change Biology*, 14, 2015-2039, 2008.
- 823 Smith, L. C., Sheng, Y., MacDonald, G. M., and Hinzman, L. D.: Disappearing Arctic Lakes,
824 *Science*, 308, 1429-1429, 2005.
- 825 Smith, N. V., Saatchi, S. S., and Randerson, J. T.: Trends in high northern latitude soil freeze and
826 thaw cycles from 1988 to 2002, *Journal of Geophysical Research: Atmospheres*, 109, D12101,
827 2004.
- 828 Sturm, M., Douglas, T., Racine, C., and Liston, G. E.: Changing snow and shrub conditions
829 affect albedo with global implications, *Journal of Geophysical Research: Biogeosciences*, 110,
830 G01004, 2005.
- 831 Sullivan, P.: Snow distribution, soil temperature and late winter CO₂ efflux from soils near the
832 Arctic treeline in northwest Alaska, *Biogeochemistry*, 99, 65-77, 2010.
- 833 Swenson, S. C. and Lawrence, D. M.: A new fractional snow-covered area parameterization for
834 the Community Land Model and its effect on the surface energy balance, *Journal of Geophysical
835 Research: Atmospheres*, 117, n/a-n/a, 2012.
- 836 Tang, J. and Riley, W. J.: Large uncertainty in ecosystem carbon dynamics resulting from
837 ambiguous numerical coupling of carbon and nitrogen biogeochemistry: A demonstration with
838 the ACME land model, *Biogeosciences Discuss.*, 2016, 1-27, 2016.
- 839 Tarnocai, C., Canadell, J. G., Schuur, E. A. G., Kuhry, P., Mazhitova, G., and Zimov, S.: Soil
840 organic carbon pools in the northern circumpolar permafrost region, *Global Biogeochemical
841 Cycles*, 23, GB2023, 2009.



- 842 Thompson, S. L., Govindasamy, B., Mirin, A., Caldeira, K., Delire, C., Milovich, J., Wickett,
843 M., and Erickson, D.: Quantifying the effects of CO₂-fertilized vegetation on future global
844 climate and carbon dynamics, *Geophysical Research Letters*, 31, L23211, 2004.
- 845 Van Wijk, M. T., Clemmensen, K. E., Shaver, G. R., Williams, M., Callaghan, T. V., Chapin, F.
846 S., Cornelissen, J. H. C., Gough, L., Hobbie, S. E., Jonasson, S., Lee, J. A., Michelsen, A., Press,
847 M. C., Richardson, S. J., and Rueth, H.: Long-term ecosystem level experiments at Toolik Lake,
848 Alaska, and at Abisko, Northern Sweden: generalizations and differences in ecosystem and plant
849 type responses to global change, *Global Change Biology*, 10, 105-123, 2004.
- 850 Wadham, J. L., Hallam, K. R., Hawkins, J., and O'Connor, A.: Enhancement of snowpack
851 inorganic nitrogen by aerosol debris, *Tellus B*, 58, 229-241, 2006.
- 852 Wahren, C. H. A., Walker, M. D., and Bret-Harte, M. S.: Vegetation responses in Alaskan arctic
853 tundra after 8 years of a summer warming and winter snow manipulation experiment, *Global
854 Change Biology*, 11, 537-552, 2005.
- 855 Wainwright, H. M., Dafflon, B., Smith, L. J., Hahn, M. S., Curtis, J. B., Wu, Y., Ulrich, C.,
856 Peterson, J. E., Torn, M. S., and Hubbard, S. S.: Identifying multiscale zonation and assessing
857 the relative importance of polygon geomorphology on carbon fluxes in an Arctic tundra
858 ecosystem, *Journal of Geophysical Research: Biogeosciences*, 120, 788-808, 2015.
- 859 Walker, D. A., Raynolds, M. K., Daniëls, F. J. A., Einarsson, E., Elvebakk, A., Gould, W. A.,
860 Katenin, A. E., Kholod, S. S., Markon, C. J., Melnikov, E. S., Moskalenko, N. G., Talbot, S. S.,
861 Yurtsev, B. A., and The other members of the, C. T.: The Circumpolar Arctic vegetation map,
862 *Journal of Vegetation Science*, 16, 267-282, 2005.
- 863 Walker, M. D., Wahren, C. H., Hollister, R. D., Henry, G. H. R., Ahlquist, L. E., Alatalo, J. M.,
864 Bret-Harte, M. S., Calef, M. P., Callaghan, T. V., Carroll, A. B., Epstein, H. E., Jónsdóttir, I. S.,
865 Klein, J. A., Magnússon, B., Molau, U., Oberbauer, S. F., Rewa, S. P., Robinson, C. H., Shaver,
866 G. R., Suding, K. N., Thompson, C. C., Tolvanen, A., Totland, Ø., Turner, P. L., Tweedie, C. E.,
867 Webber, P. J., and Wookey, P. A.: Plant community responses to experimental warming across
868 the tundra biome, *Proceedings of the National Academy of Sciences of the United States of
869 America*, 103, 1342-1346, 2006.
- 870 Warscher, M., Strasser, U., Kraller, G., Marke, T., Franz, H., and Kunstmann, H.: Performance
871 of complex snow cover descriptions in a distributed hydrological model system: A case study for



- 872 the high Alpine terrain of the Berchtesgaden Alps, *Water Resources Research*, 49, 2619-2637,
873 2013.
- 874 Welker, J. M., Fahnestock, J. T., and Jones, M. H.: Annual CO₂ Flux in Dry and Moist Arctic
875 Tundra: Field Responses to Increases in Summer Temperatures and Winter Snow Depth,
876 *Climatic Change*, 44, 139-150, 2000.
- 877 Wiggins, I. L.: The distribution of vascular plants on polygonal ground near Point Barrow,
878 Alaska, *Stanford University Contributions of the Dudley Herbarium*, 4, 41-52, 1951.
- 879 Williams, M. W., Hood, E., and Caine, N.: Role of organic nitrogen in the nitrogen cycle of a
880 high-elevation catchment, Colorado Front Range, *Water Resources Research*, 37, 2569-2581,
881 2001.
- 882 Williams, T. and Flanagan, L.: Effect of changes in water content on photosynthesis,
883 transpiration and discrimination against ¹³C and ¹⁸O in *Pleurozium* and *Sphagnum*,
884 *Oecologia*, 108, 38-46, 1996.
- 885 Wilkening, M., Juday, G. P., Barber, V. A., and Zald, H. S. J.: Recent climate warming forces
886 contrasting growth responses of white spruce at treeline in Alaska through temperature
887 thresholds, *Global Change Biology*, 10, 1724-1736, 2004.
- 888 Wu, Y., Hubbard, S. S., Ulrich, C., and Wulschleger, S. D.: Remote Monitoring of Freeze–
889 Thaw Transitions in Arctic Soils Using the Complex Resistivity Method, *gsvadzone*, 2013. 2013.
- 890 Xu, X., Riley, W. J., Koven, C. D., Billesbach, D. P., Chang, R. Y. W., Commene, R.,
891 Euskirchen, E. S., Hartery, S., Harazono, Y., Iwata, H., McDonald, K. C., Miller, C. E., Oechel,
892 W. C., Poulter, B., Raz-Yaseef, N., Sweeney, C., Torn, M., Wofsy, S. C., Zhang, Z., and Zona,
893 D.: A multi-scale comparison of modeled and observed seasonal methane emissions in northern
894 wetlands, *Biogeosciences*, 13, 5043-5056, 2016.
- 895 Zeng, N., Qian, H., Munoz, E., and Iacono, R.: How strong is carbon cycle-climate feedback
896 under global warming?, *Geophysical Research Letters*, 31, L20203, 2004.
- 897 Zeng, X. and Decker, M.: Improving the Numerical Solution of Soil Moisture–Based Richards
898 Equation for Land Models with a Deep or Shallow Water Table, *Journal of Hydrometeorology*,
899 10, 308-319, 2009.
- 900 Zhu, Q., Iversen, C. M., Riley, W. J., Slette, I. J., and Vander Stel, H. M.: Root traits explain
901 observed tundra vegetation nitrogen uptake patterns: Implications for trait-based land models,
902 *Journal of Geophysical Research: Biogeosciences*, 121, 3101-3112, 2016a.



903 Zhu, Q. and Riley, W. J.: Improved modelling of soil nitrogen losses, *Nature Clim. Change*, 5,
904 705-706, 2015.

905 Zhu, Q., Riley, W. J., Tang, J., and Koven, C. D.: Multiple soil nutrient competition between
906 plants, microbes, and mineral surfaces: model development, parameterization, and example
907 applications in several tropical forests, *Biogeosciences*, 13, 341-363, 2016b.

908 Zona, D., Lipson, D. A., Zulueta, R. C., Oberbauer, S. F., and Oechel, W. C.: Microtopographic
909 controls on ecosystem functioning in the Arctic Coastal Plain, *Journal of Geophysical Research:*
910 *Biogeosciences*, 116, G00I08, 2011.